UNIVERSITAT POLITÈCNICA
DE CATALUNYA

GEOPLEX: GSSA and VSS Models

C. Batlle, D. Biel, E. Fossas, C. Gaviria, R. Griñó, and S. Martínez

IOC-DT-P-2004-21
Octubre 2004

Institut d'Organització i Control
de Sistemes Industrials

GSSA and VSS models

C. Batlle[1,2,5], D. Biel[1,4], E. Fossas[3,5], C. Gaviria[5], R. Griñó[3,5] and S. Martínez[1,2]
[1]EPSEVG, [2]MAIV, [3]ESAII, [4]EE, and [5]IOC
Technical University of Catalonia

Contents

1 Introduction

This report describes some aspects of the theory of Variable Structure Systems (VSS). It starts with the state-of-the-art classical methods of control and evolves to a description based on average port hamiltonian models.

In the framework of GEOPLEX, VSS appear due to the fact that some of the plants of interest are controlled using power converters, which are systems with switches, changing between several circuit topologies.

In Section 2, the basic ideas of Sliding Mode Control (SMC) for VSS are presented, and a somewhat detailed exposition of its application to the control of a power converter is given.

Most of Section 3 is unpublished material, describing some preliminary results about the relation between (generalized) averaging and the port hamiltonian description. The fundamentals of State Space Averaging (SSA) and Generalized State Space Averaging (GSSA) are presented, and averaged port hamiltonian models for second order power converters are introduced. There is a summary of some rigorous mathematical results about GSSA, and a relationship between the hamiltonians of the GSSA models and the original hamiltonian is stablished for systems with quadratic hamiltonian functions.

2 Sliding mode control

2.1 Introduction

The use of sliding-control techniques in variable structure systems (VSS) improves considerably the dynamic behavior of these systems compared to the conventional control method. The dynamic performances of VSS in sliding regime are basically a fast transient response without overshoot and a low sensitivity to external perturbations.

Switching converters constitute an important case of VSS, and different sliding mode strategies to control this class of circuits have been reported in the last years [5], [21]. Depending on the task they are supposed to do, and the control algorithm, they are nonlinear time-varying dynamical systems. They can be modelled as variable structure systems because of the abrupt topological changes that the circuit, commanded by a discontinuous control action, undergoes. They constitute a natural field of application of Sliding Mode Control techniques which is based on the following two main concepts:

- to define a surface, i.e. a relationship between state variables, in such a way that, if trajectories slide on this surface, a previously stated behavior (for instance reaching an equilibrium point) is achieved.
- to design an appropriate control law forcing this surface to be an attractor and a dynamically invariant set.

2.1.1 Definitions

Let us consider a single input dynamical system given by

$$\dot{x} = f(x) + ug(x) \tag{1}$$

where $x \in U$, an open set of $\mathbb{R}^n$, f and g are smooth vector fields on U with $g(x) \neq 0$ everywhere, and $u : U \longrightarrow \mathbb{R}$ is the control input.

Let Σ be a submanifold in U defined by a smooth function $s : U \longrightarrow \mathbb{R}$, namely

$$\Sigma = \{x \in U \mid s(x) = 0\} \tag{2}$$

where $(\text{grad } s)(x) \neq 0$, $\forall x \in U$ and $\Sigma \cap U \neq \emptyset$ are assumed.

As for the input, let us take u defined by

$$u = \begin{cases} u^+(x) & \text{if } s(x) > 0 \\ u^-(x) & \text{if } s(x) < 0 \end{cases} \tag{3}$$

where both u^+ and u^- are smooth functions of x. There is no loss of generality in assuming $\langle \text{grad } s, g \rangle > 0$.

Finally, let $\phi(x,t)$ be the trajectory of the dynamical system defined by (1), (2) and (3) with initial conditions $x(0) = x$. It is worth remarking that the former dynamical system is discontinuous on $H = 0$; thus the standard results on differential equations do not apply. We will deal with this subject later; let us assume for the moment the existence and uniqueness of trajectories.

Definition: Σ is said to be a sliding surface for the dynamical system defined by (1), (2) and (3) if there exists θ, an open set in U containing Σ, in such a way that $\forall x \in \theta \setminus \Sigma$, one of the following conditions holds:

(i) There exists a finite time $t_s > 0$ such that

$$s(\phi(x,t)) \neq 0 \quad 0 \leq t < t_s \quad \text{and} \quad s(\phi(x,t)) = 0 \quad t \geq t_s.$$

(ii) There exist t_s and $\hat{t}_s$, $0 < t_s < \hat{t}_s < \infty$ such that

$$s(\phi(x,t)) \neq 0 \quad 0 \leq t < t_s \quad \text{and} \quad s(\phi(x,t)) = 0 \quad t_s \leq t < \hat{t}_s.$$

and $\phi(x, \hat{t}_s) \in \partial(\Sigma \cap U)$

Roughly speaking, the trajectories starting in a neighborhood of Σ must fall on Σ and remain there (case 1) or, should one escape, it must go through $\partial(\Sigma \cap U)$. As a first consequence of the definition, two questions arise, namely

(i) Existence. Which conditions on f, g, u and Σ, if any, guarantee that Σ be a sliding surface?

(ii) Ideal sliding dynamics. Note that the dynamics defined by (1), (2) and (3) do not consider Σ; however, if Σ is a sliding surface, it is dynamically invariant. Then the question is which vector field governs the system on Σ.

Both problems are solved below.

2.1.2 Method of equivalent control and ideal sliding dynamics

Definition: Let us define equivalent control as the control law, $u_{eq} : U \to \mathbb{R}$, which makes Σ an invariant manifold for the dynamical system defined in (1), that is to say, u_{eq} is such that the vector field $f + gu_{eq}$ is tangent to Σ. This results in

$$\langle \text{grad } s, f + g\ u_{eq} \rangle = 0 \tag{4}$$

where $\langle \cdot, \cdot \rangle$ denotes the standard scalar product, and thus

$$u_{eq} = -\frac{\langle \text{grad } s, f \rangle}{\langle \text{grad } s, g \rangle} \tag{5}$$

As it is proved in [6], a paper by Filipov on differential equations with discontinuous right-hand side, ideal sliding dynamics, i.e. the dynamics on Σ, are governed by the vector field

$$f(x) + g(x)\ u_{eq}(x)$$

Notice that a necessary condition for the existence of equivalent control is $\langle \text{grad } s, g \rangle \neq 0$. This equivalent control makes the sliding surface dynamically invariant. Hence, system trajectories reaching Σ slide on it. Ideal sliding dynamics remains to be studied, particularly by computing possible equilibrium points and determining whether they are stable or not.

2.1.3 Control law and sliding motion

As far as existence is concerned, two results, depending on whether u^+ and u^- are fixed or not, are given below.

Proposition: Σ is a sliding surface for the dynamical system defined by (1), (2) and (3) if and only if there exists θ, a neighbourhood of Σ, such that

$$\left.\begin{array}{l} \dfrac{d}{dt} s(\phi(x,t)) < 0 \quad \text{if } s(\phi(x,t)) > 0 \\[2ex] \dfrac{d}{dt} s(\phi(x,t)) > 0 \quad \text{if } s(\phi(x,t)) < 0 \end{array}\right\}$$

Remark
We consider derivatives of s along the trajectories of the vector field $f(x) + ug(x)$ for the values of u defined in (3). These conditions may also be written as

$$\left.\begin{array}{l} \lim\limits_{s \to 0^+} L_{f+gu^+} s(x) < 0 \\[2ex] \lim\limits_{s \to 0^-} L_{f+gu^-} s(x) > 0 \end{array}\right\} \tag{6}$$

where $L_{f+gu^+} s(x)$ denotes the directional derivative of the scalar function s with respect to the vector field $f + gu$ at point x. That is to say, the change rate of the scalar surface coordinate function $s(x)$, measured in the direction of the controlled field, is such that a crossing of the surface is guaranteed.

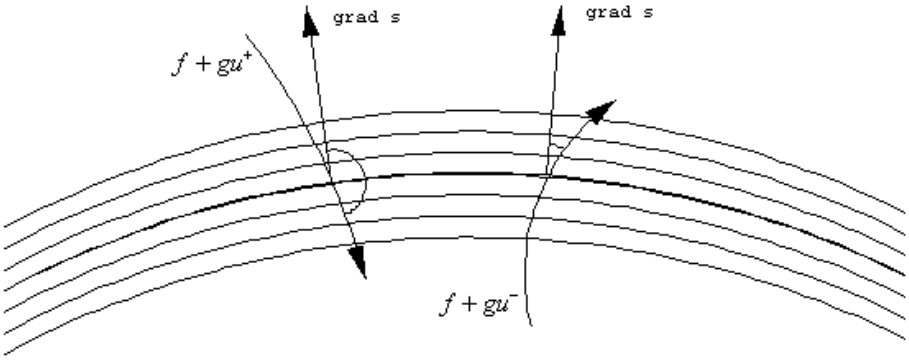

Figure 1: A graphic interpretation of the conditions given in (6).

These conditions are equivalent to

$$\left.\begin{array}{l} \lim\limits_{s\to 0^+} \langle \text{grad } s, f + gu^+ \rangle < 0 \\ \lim\limits_{s\to 0^-} \langle \text{grad } s, f + gu^- \rangle > 0 \end{array}\right\} \tag{7}$$

The geometrical meaning is that on Σ the projections of the controlling vector fields $f + gu^+$ and $f + gu^-$ on (grad s) are of the opposite sign, and hence the controlled fields locally point towards the surface Σ (Figure 1). In practice, sliding motion is not attainable; imperfections such as hysteresis, delays, sampling and unmodelled dynamics will result in a chattering motion in a neighbourhood of the sliding surface, as it has been schematized in Figure 2. Such a real model will usually lie in the field of ordinary differential equations, and therefore there is no need for Filipov's theory. Moreover, if the control functions u^+ and u^- can be designed arbitrarily, the next proposition gives a very simple condition for Σ to be a sliding surface.

Proposition: A necessary and sufficient condition for the existence of control functions u^+ and u^- making Σ be a sliding surface is

$$\langle \text{grad } s, g \rangle \neq 0 \tag{8}$$

which is known as the *transversality condition*.

The proof is easy and can be found in [21] where this subject is widely considered. The cornerstone of the proof is to take the function s^2 as a Lyapunov function.

2.2 The single phase back-to-back converter.

2.2.1 Introduction

The most popular AC/DC/AC power conversion is performed by means of a PWM rectifier-inverter system with dc voltage link. This approach makes use of a capacitor (normally electrolytic, bulky and expensive) in the DC link, which causes decoupling between the rectifier and the inverter. Some of the latest studies on AC/DC/AC power conversion deal with the strategies to reduce the dc-link capacitors [14]-[11].

The desired unity power factor constitutes one of the rectifier requirements. In the same way, the AC output voltage has to be in phase with the AC input voltage and with a reduced THD factor. The control technique mostly used to drive the two decoupling converters is based on the usual and well-known linearisation technique applied to the design of PWM control schemes. Sliding-mode control techniques have been proposed as an alternative to PWM control strategies in DC-DC switching regulators since

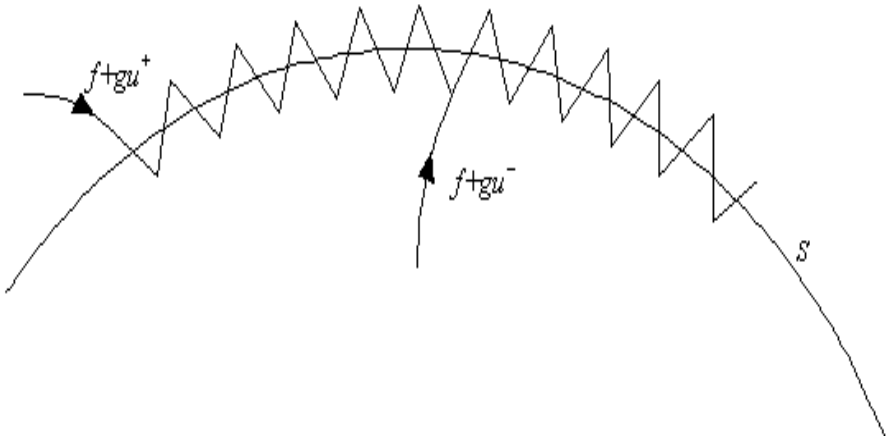

Figure 2: Chattering.

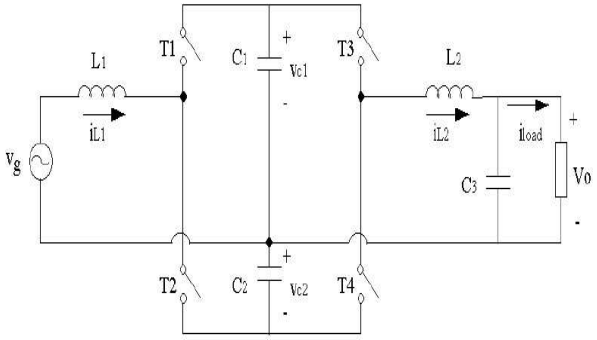

Figure 3: Single-phase inverter with rectifier.

they make these systems very robust to perturbations, namely variations of the input voltage and/or in the load [20]-[24]. These techniques have also been applied to the design of high-efficiency inverters, where a switching DC-DC converter is forced to track an external sinusoidal reference by means of an appropriate sliding-mode control action [7],[4],[1].

We propose two switching surfaces and their respective control policies to track the output voltage tracking and to guarantee unity power factor in a single-phase inverter with input rectifier, respectively. Whereas the former sliding surface is a linear combination of the output voltage error and its derivative, the latter results in a surface not only depending on time, but on the energy balance as well. This energy balance is measured at each period of the AC input voltage. The problem we deal with can be redefined as the design of appropriate surfaces in order to make the outputs of the system reach zero as a stable equilibrium point. One of these surfaces has to be iteratively defined, otherwise the zero dynamics is not stable.

2.2.2 The single-phase inverter with input rectifier. State equations

Let us consider the single-phase inverter with phase controlled rectifier acting as power supply depicted in Figure 3, where half bridges have been employed to ensure the bipolarity of the AC output.

The power system, considering ideal switches and lossless reactive elements, can be represented by

the set of differential equations

$$L_1 \frac{di_{L_1}}{d\tau} = (v_g - v_{C_1}) + u_2(v_{C_1} + v_{C_2}) \quad (9)$$

$$C_1 \frac{dv_{C_1}}{d\tau} = (i_{L_1} - i_{L_2}) + u_1 i_{L_2} - u_2 i_{L_1} \quad (10)$$

$$L_2 \frac{di_{L_2}}{d\tau} = (v_{C_1} - v_o) - u_1(v_{C_1} + v_{C_2}) \quad (11)$$

$$C_2 \frac{dv_{C_2}}{d\tau} = u_1 i_{L_2} - u_2 i_{L_1} \quad (12)$$

$$C_3 \frac{dv_o}{d\tau} = i_{L_2} - i_{load} \quad (13)$$

where, as can be seen in Figure 3, i_{L_1} and i_{L_2} are currents through the inductors, i_{load} is the current through the load, v_{C_1}, v_{C_2} and v_o are voltages in the capacitors, L_1 and L_2 are inductance values, C_1, C_2 and C_3 are capacitance values, $v_g = b\sin(2\pi f_0 \tau)$ is the input voltage, and $u_1,\ u_2$ are the control signals, which belong to the discrete set $\{0, 1\}$; u_1 drives (T_3, T_4) and u_2 drives (T_1, T_2).

For a systematic study, it is convenient to consider a dimensionless model obtained by the change of variables

$$\left.\begin{array}{rclrcl} x_1 &=& \frac{v_{C_1}+v_{C_2}}{b} & x_2 &=& \frac{v_{C_1}-v_{C_2}}{b} \\ y_1 &=& \frac{i_{L_1}}{b}\sqrt{\frac{L_1}{C_1}} & y_2 &=& \frac{i_{L_2}}{b}\sqrt{\frac{L_1}{C_1}} \\ x_3 &=& \frac{v_o}{b} & y_{load} &=& \frac{i_{load}}{b}\sqrt{\frac{L_1}{C_1}} \\ t &=& \frac{\tau}{\sqrt{L_1 C_1}} & f &=& \sqrt{L_1 C_1} f_0 \\ v_1 &=& 1 - 2u_1 & v_2 &=& 1 - 2u_2 \\ h &=& \frac{v_g}{b} = \sin(2\pi f t) & & & \end{array}\right\}$$

Namely,

$$\frac{dy_1}{dt} = h - \frac{x_2}{2} - \frac{v_2 x_1}{2} \quad (14)$$

$$\frac{dx_1}{dt} = v_2 y_1 - v_1 y_2 \quad (15)$$

$$\frac{dy_2}{dt} = L\left(\frac{v_1 x_1}{2} + \frac{x_2}{2} - x_3\right) \quad (16)$$

$$\frac{dx_2}{dt} = y_1 - y_2 \quad (17)$$

$$\frac{dx_3}{dt} = C\,(y_2 - y_{load}) \quad (18)$$

where $L = \frac{L_1}{L_2}$, $C = \frac{C_1}{C_3}$ and $C_1 = C_2$ is assumed.

Also notice that the energy stored in the plant can be measured by

$$E = y_1^2 + \frac{x_1^2}{2} + \frac{x_2^2}{2} + \frac{y_2^2}{L} + \frac{x_3^2}{C} \quad (19)$$

and that

$$\frac{dE}{dt} = 2\,[y_1 h - y_{load} x_3] \quad (20)$$

describes the energy balance.

2.2.3 Design and analysis

The requirements which the AC/DC/AC converter have to meet are:

- the input current must be in phase with the input voltage (unity power factor),
- the output voltage provided to the load must be a sinus wave of 50Hz of frequency and $b = 220\sqrt{2}$V of amplitude.
- the voltage of the bus, represented by the dimensionless variable x_1, should remain in a neighborhood of a nominal value x_1^*. This is equivalent to $|E - E^*| < \rho$, where E^* is the nominal energy and ρ the radius of the neighborhood.

The first and second demands can respectively be written as

(i) $\forall t \in [nT, (n+1)T), \quad y_1(t) - k_n h(t) = 0.$

(ii) $\forall t \geq t_0, \quad x_3(t) - h(t) = 0$

where k_n is constant for all $t \in [nT, (n+1)T)$ and $T = f^{-1}$. Concerning the third demand, it will be achieved by an appropriate design of the coefficient k_n.

In order to design sliding-mode controllers in such a way that the previous tracking conditions are satisfied, remark that the relative degrees of $y_1 - k_n h$ and $x_3 - h$ with respect to (v_1, v_2) are $(2, 1)$ and $(2, 3)$, respectively.

Then, let us define as sliding surfaces:

$$\sigma_1 := y_1 - k_n h = 0 \tag{21}$$

$$\sigma_2 := (x_3 - h) + \kappa \frac{d(x_3 - h)}{dt} = 0 \tag{22}$$

It is straightforward to prove that

$$\frac{\partial \sigma_1}{\partial v_1} = 0 \qquad \frac{\partial \sigma_2}{\partial v_2} = 0,$$

so σ_1 will tend to zero under an appropriate design of v_2 irrespective of the value of v_1, respectively for σ_2, v_1 and v_2.

The control law

$$v_1 = \begin{cases} +1 & \text{if } \sigma_2 < 0 \\ -1 & \text{if } \sigma_2 > 0 \end{cases} \tag{23}$$

$$v_2 = \begin{cases} +1 & \text{if } \sigma_1 < 0 \\ -1 & \text{if } \sigma_1 > 0 \end{cases} \tag{24}$$

locally qualifies σ_1^2 and σ_2^2 as Lyapunov functions; therefore, (21) and (22) tend to zero in the controlled system, and the desired behaviour is ensured. As in [4], the performance of equation (22) guarantees a robust dynamics with respect to load disturbances.

As to the value of k_n, let us assume sliding motion on σ_1 and on σ_2, remember that $h(t) = \sin(2\pi f t)$ and solve $E(t)$ from equation (20) for $t \in [nT, (n+1)T)$; then

$$\begin{aligned} E(t) &= E(nT) + 2k_n \left[\frac{t - nT}{2} - \frac{\sin(4\pi f t)}{8\pi f} \right] - \\ &- 2 \int_{nT}^{t} y_{load}(\tau) h(\tau) d\tau \end{aligned} \tag{25}$$

Let γ_n be the average load defined by

$$\gamma_n = 2f \int_{nT}^{(n+1)T} y_{load}(\tau) h(t) dt$$

The energy of the system at $t = (n+1)T$ is

$$E_{n+1} = E((n+1)T) = E_n + (k_n - \gamma_n)T \tag{26}$$

resulting in a discrete dynamical system with input k_n and output E_n. Under the hypotheses that $\gamma_n = \gamma_{n-1}$ almost every time, γ_n can be estimated through $E_n - E_{n-1}$. Namely,

$$(E_n - E_{n-1}) - T k_{n-1} = -T\gamma_{n-1}$$

and equation (26) results in

$$E_{n+1} - E_n = T(k_n - k_{n-1}) + E_n - E_{n-1}$$

Then, let us define

$$k_n = k_{n-1} - \frac{E_n - E_{n-1}}{T} + \frac{(1+\varepsilon)(E^* - E_n)}{T} \tag{27}$$

which is equivalent to

$$k_n = \gamma_{n-1} + \frac{(1+\varepsilon)(E^* - E_n)}{T} \tag{28}$$

Equations (26) and (28) yield

$$(z+\varepsilon)\mathcal{Z}(E) = (1+\varepsilon)E^* - T(z-1)\mathcal{Z}(\gamma)$$

which states that for $-1 < \varepsilon < 1$ the solution E_n of equation (26) is stable. E_n reaches the steady state E^* if γ_n does so too.

E_n can be computed from equation (19) presuming the initial condition is known. Finally, as one can assume the initial conditions hold $\sigma_1 = 0$ and $\sigma_2 = 0$, $E_0 = E(0)$ is

$$\frac{x_1^2(0)}{2} + \frac{y_2^2(0)}{L} \tag{29}$$

2.3 Quasi-sliding mode control implementations in switching systems

This subsection deals with a comparative study of several sliding mode control implementations in switching systems. The switching frequency is required to be stable and synchronous for this type of systems, this resulting in the hardest requirements for non-standard implementation strategies. The use of fixed and variable bandwidth hysteresis comparators, the addition of an external synchronous signal and the use of the equivalent control as duty cycle (with and without zero-order-hold) are considered here and compared to the Zero Average Dynamics control strategy. Comparisons are referred to a Buck power converter in tracking signal tasks. The paper includes simulations and experimental results. The ZAD fulfils the requirement of fixed frequency and exhibits similar robustness properties to sliding mode control.

2.3.1 Introduction

The most important characteristics of sliding control is its robustness in the presence of parameter variations and external perturbations [23], [20]. It is worth noting that this theory presumes an infinite switching frequency when the system operates in sliding mode, and that actual switches cannot commute at infinite frequency; at any rate, higher switching frequencies become harmful in some of the applications. In power electronics for instance, the higher the switching frequency, the higher the losses in the converter. Consequently, actual sliding mode controls operate at high, finite, possibly variable frequency which results in a chattering around the sliding surface.

Classical approaches for eliminating chattering are based on the substitution of the discontinuous control action for a continuous one in a strip containing the sliding surface ("boundary layer"). As a result, ripple disappears. Several proposals in this line can be found in the literature. They approximate the sign function through piecewise linear or sigmoidal functions. The sliding regime disappears using these approximations, and the trajectories evolve close to ideal sliding dynamics. As reported in [25], for these approximations, a full knowledge of parasitics dynamics is required so that it can be considered in the controller design to avoid instabilities. Furthermore, defining a continuous signal from a discontinuous one which, in turn, is pulse-with-modulated to obtain a discontinuous control action, like the actual control action in power electronics, does not seem to be a good option.

Thus, several questions arise: first, what options does an engineer have, in order to implement a control action based on sliding control theory? Second, what are the best methodology and the optimal implementation? Third, what criteria must be followed to chose the implementation?

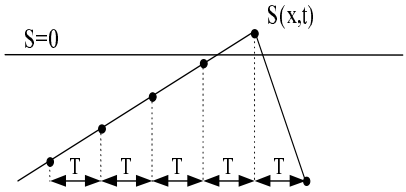

Figure 4: Loosing switching opportunities due to the use of a Zero Order Hold

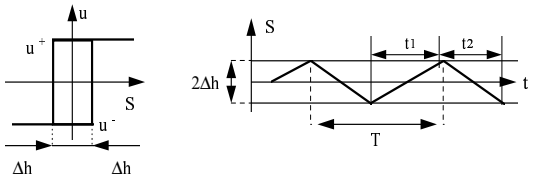

Figure 5: Hysteresis cycle and sliding surface dynamics

2.3.2 Sliding control mode implementation in switching converters

Let $\dot{x} = f(x) + g(x) \cdot u$ be a single input single output, autonomous, non linear system controlled trough a sliding surface $S(x,t) = 0$ and an appropriate control law. Let us assume that the system behavior is given by the ideal sliding dynamics:

$$\left\{ \begin{array}{rcl} S(x,t) & = & 0 \\ \dot{x} & = & f(x) + g(x)ueq \end{array} \right. \tag{30}$$

where ueq is the equivalent control and, in this case, the switching frequency is assumed to be infinite.

As the actual system cannot reach the ideal sliding dynamics, the actual dynamics is characterized by

$$\left\{ \begin{array}{rcl} S(x,t) & \approx & 0 \\ \dot{x} & = & f(x) + g(x)\mu(x) \end{array} \right. , \tag{31}$$

where, in the particular case of having a fixed switching frequency

$$\mu(x) = \left\{ \begin{array}{ll} u^+ & \text{if} \leq t < (k+d_k)T \\ u^- & \text{if } (k+d_k)T \leq t < (k+1)T \end{array} \right. . \tag{32}$$

The duty cycle d_k, or in general $d_k(x,t)$, defines the control action. Usually, it is obtained by pulse with modulation of a processed system output. There are other control strategies providing fixed frequency switching, for example, in [21] the duty cycle is defined as the equivalent control evaluated at the beginning of the control period $d(k) = \frac{ueq(t)-u^-}{u^+-u^-}\Big|_{t=kT}$. The weak point of this strategy lies in the need to know the system parameters, this resulting in a loss of system robustness.

The use of a Zero Order Hold to synchronize the signal control changes does not seem to be an appropriate option since commutations are gradually lost as the sampling period increases, as sketched in Figure 4.

Authors in [2]-[15] propose the addition of an hysteresis cycle to the sliding mode control comparator, as shown in Figure 5.

The switching frequency f_s can be derived as follows:

$$\left\{ \begin{array}{l} \frac{dS}{dt}\big|_{u=u^+} = \frac{2\Delta h}{t1} \\ \\ \frac{dS}{dt}\big|_{u=u^-} = -\frac{2\Delta h}{t2} \end{array} \right. ; \quad \left\{ \begin{array}{l} t1 = \frac{2\Delta h}{\frac{\partial S}{\partial x} g(x)(u^+ - ueq)} \\ \\ t2 = \frac{2\Delta h}{\frac{\partial S}{\partial x} g(x)(u^- - ueq)} \end{array} \right. \tag{33}$$

as a conclusion, we have

$$f_s = \frac{1}{t1+t2} = \frac{\partial S}{\partial x} \frac{g(x)}{2\Delta h} \frac{(u^- - ueq)(ueq - u^+)}{(u^- - u^+)} \tag{34}$$

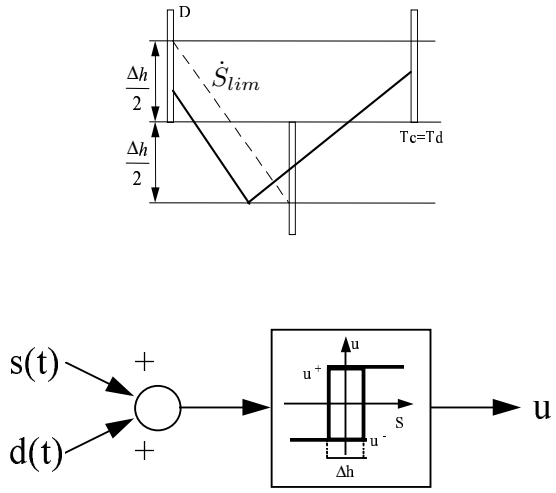

Figure 6: Adding an external signal to the sliding surface.

Note that the switching frequency is bounded but variable (not fixed) for time dependent equivalent controls. In this case, the maximum switching frequency is

$$f_{s\max} = \frac{\partial S}{\partial x}\frac{g(x)}{2\Delta h}\left.\frac{(u^- - ueq(t))(ueq(t) - u^+)}{(u^- - u^+)}\right|_{\max} \tag{35}$$

It is worth noticing that the processing time of the analog or digital processor subsystem has not been taken into account. This processing time will affect the resulting dynamics in the case it cannot be neglected in comparison with the switching period.

Several approaches, [17]-[13], consider a variable bandwidth hysteresis cycle, the implementation of which depends on the system parameters and is also complex.

Note that

$$\Delta h = \mu\frac{(u^- - ueq)(ueq - u^+)}{(u^- - u^+)} \rightarrow f_s = \frac{1}{2\mu}\frac{\partial S}{\partial x}g(x) \tag{36}$$

and the switching frequency can be stabilized.

Other electronic implementations of quasi-sliding controls are reported in [19]-[16]. The fixed switching frequency is forced by an external signal, as can be seen in Figure 3.

In this approach, a successful design demands first, to achieve commutation (which means $D > \frac{\Delta h}{2}$), second $Td < Tcmax$ (with hysteresis cycle $fd > f_{s\max}$), third to avoid double commutations and to achieve fixed frequency, that is:

$$\dot{S}\lim \geq \dot{S}_{\max} \rightarrow \Delta h \geq \frac{1}{4f_s}\frac{\partial S}{\partial x}g(x)(u^+ - u^-) \tag{37}$$

Among the problems detected in the method, we can point out the difficult tuning of the commutation system, the need for an external signal and the effect of the synchronism signal on the resulting dynamics.

Finally, in [9], [8] the duty cycle is defined so that the average of the sliding surface is zero in each commutation period; that is to say, the controller guarantees

$$\langle S(x,t)\rangle = \frac{1}{T}\cdot\int_{KT}^{(K+1)T} S(x,\tau)\cdot d\tau = 0 \tag{38}$$

The control algorithm is defined in Table I, and the behaviour of the sliding surface is outlined, using the definitions given in Table I, in Figure 7. Note that the duty cycle only depends on the value of the switching surface function $S(x,t)$ and its derivatives.

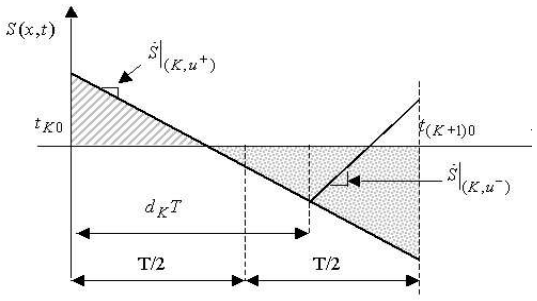

Figure 7: Zero Average Dynamics control.

2.3.3 Comparative study of the implementation methods

With the aim of comparing the aforementioned "quasi-sliding" implementation strategies, a sliding control for solving a tracking problem in a buck power converter is designed. The signal to be tracked is a sinus wave. Simulation results are obtained for each implementation strategy through Matlab-Simulink and then compared.

The buck converter is widely used in DC-DC and DC-AC power electronic systems. Since the efficiency of the conversion and the output signal spectrum strongly depend on the switching frequency, it is necessary to establish procedures for managing it. For this reason, in industrial applications, an upper bound on the switching frequency is a specification the control system must fulfil. Several reports and proposals on this issue can be found in the literature. Some of them try to restrict or to predetermine the actual switching frequency of sliding mode controllers. Contributions based on including a fixed hysteresis bandwidth achieving a limited switching frequency are reported in [4], [15].

Starting from implementations based on an hysteresis cycle, some authors aim to combine the characteristic robustness of the sliding control mode with fixed switching frequency fulfilments, either using a variable bandwidth hysteresis cycle [17]-[13] or adding a synchronism signal external to the system [19], [16].

The buck converter can be modelled in state-space by:

$$\frac{d}{dt}\begin{pmatrix} i \\ v \end{pmatrix} = \begin{pmatrix} 0 & -\frac{1}{L} \\ \frac{1}{C} & -\frac{1}{RC} \end{pmatrix}\begin{pmatrix} i \\ v \end{pmatrix} + \begin{pmatrix} \frac{E}{L} \\ 0 \end{pmatrix} u; \tag{39}$$

where $u \in \{-1, 1\}$. As in [4], the sliding surface is defined by

$$S(x,t) = k_1 \cdot (Vref(t) - v) + k_2 \cdot \left(\frac{dVref(t)}{dt} - \frac{dv}{dt}\right) \tag{40}$$

which, together with the control strategy

$$u = \begin{cases} +1 & \text{if } S(x,t) > 0 \\ -1 & \text{if } S(x,t) < 0 \end{cases} \tag{41}$$

provides the specified ideal sliding dynamics, namely $v = Vref(t) = A\sin(2\pi ft)$.

The simulation parameters are: $E = 50$V, $L = 1.5$mH, $C = 60\mu$F, $R = 20\Omega$, $f = 50$. The integrator is a $5 \cdot 10^{-8}$ fixed step Runge-Kutta 4-5.

Figures 8 and 9 show the signal errors[1] when the sliding control law is implemented using a hysteresis cycle. $\Delta h = 0.5$ and $\Delta h = 1$ have been considered in the simulation, corresponding to a maximum switching frequency of 44kHz and 22.5kHz, respectively.

Figures 10 and 11 depict the performance of the sliding surface $S(x,t)$ and the voltage error when an external signal of frequency 20kHz and amplitude 1.2 is added to $S(x,t)$ and the hysteresis cycle is $\Delta h = 0.6$. As can be seen, the error is high compared to the one obtained in the previous case.

Results for a controller based on Zero Average Dynamics at 20kHz do not much differ from the ones obtained by a hysteresis cycle (the error dynamics is displayed in Figure 13). Figure 12, in turn, shows

[1] $error = Vref(t) - v(t)$

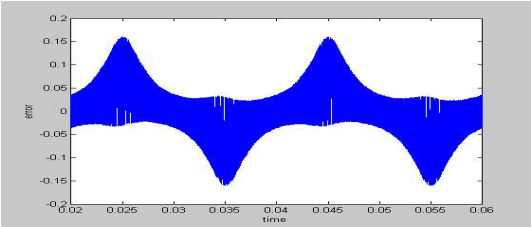

Figure 8: Voltage error when a fixed hysteresis cycle is used. $\Delta h = 0.5$

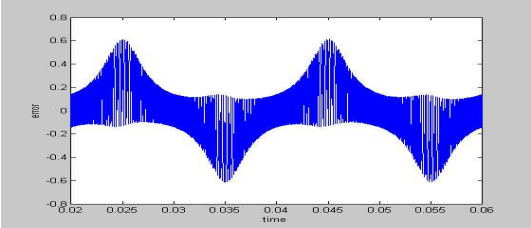

Figure 9: Voltage error with a fixed hysteresis cycle. $\Delta h = 1$.

the performance of the function $S(x,t)$. As can be seen in Figure 12, the enveloping of the function $S(x,t)$ practically coincides with the values of the hysteresis cycle obtained in case that a technique based on a variable bandwidth hysteresis cycle and a fixed switching frequency of 20kHz were used. The best result are obtained with a Pulse Width Modulation (see Figures 14 and 15) which defines the duty cycle by comparing the equivalent control with a triangular signal. Specifically, the switching time is given by the signals intersection $0.5(1+u_{eq}(t))$ and t/T, T being the switching period. The enveloping of the function $S(x,t)$ coincides again with the one that is obtained with a technique based on a variable duty cycle and a fixed switching frequency of 20kHz. Unfortunately, this method depends on the system parameters; thus, it is not applicable in practice. The achieved results using a $T-$period Zero Order Hold in series with the equivalent control $d(k) = ueq(t)|_{t=kT}$ are depicted in Figures 16 and 17. If these Figures are compared with Figures 14 and 15, the negative effect of the sampling in the control action can be observed.

When evaluating the system at a frequency of 10kHz the results worsen, see Figures 18-23. As expected, this effect is stronger in those methods which require a Zero Order Hold. In spite of this, the ZAD method provides a maximum error of 2.5% with respect to the output signal amplitude. This is the same error obtained with the strategy that uses the equivalent control and the Zero Order Hold. These results show that sampling and Zero Order Holding prevent the enveloping of the function $S(x,t)$ from coinciding with the value of the hysteresis cycle obtained if a technique based on a variable bandwidth hysteresis cycle and a 10kHz fixed switching frequency were established.

2.3.4 Experimental results

Experimental results obtained using the ZAD technique in an electronic prototype, using simulation parameters, are presented in this subsection. The switching frequency was set to 23kHz and the control algorithm was programmed in a digital logic FPGA (XC4010E-3-PC84) device, which solves the duty cycle in the 6.3% of the switching period in the worst case. This allows us to assume, in practice, that

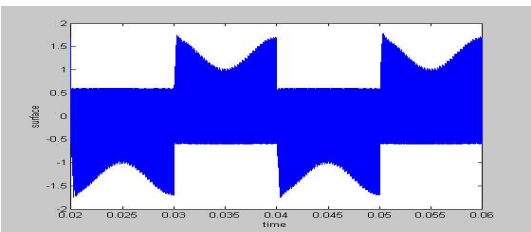

Figure 10: $S(x,t)$ with a fixed hysteresis cycle and a 20kHz frequency external signal.

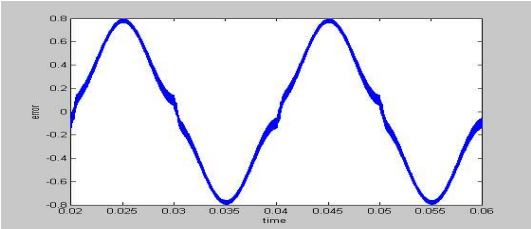

Figure 11: Voltage error with a fixed hysteresis cycle and a 20kHz frequency external signal.

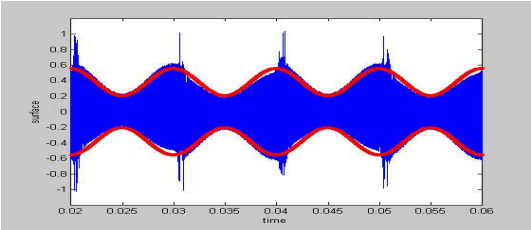

Figure 12: $S(x,t)$ with a ZAD (20kHz).

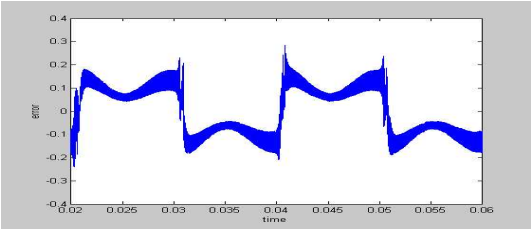

Figure 13: Voltage error with ZAD (20kHz).

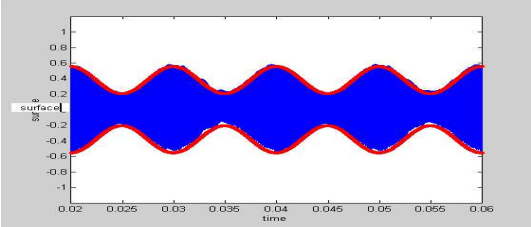

Figure 14: $S(x,t)$ using the equivalent control -without ZOH- as duty cycle (20kHz).

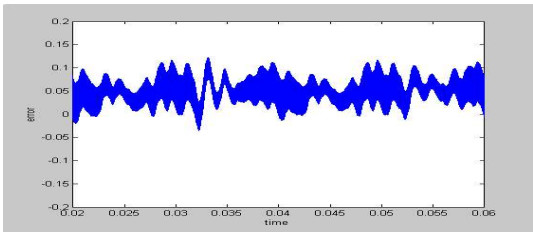

Figure 15: Voltage error using the equivalent control -without ZOH- as duty cycle (20kHz).

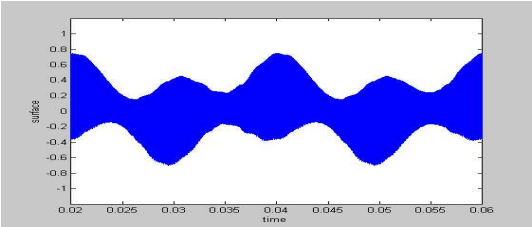

Figure 16: $S(x,t)$ using the equivalent control -with ZOH- as duty cycle (20kHz).

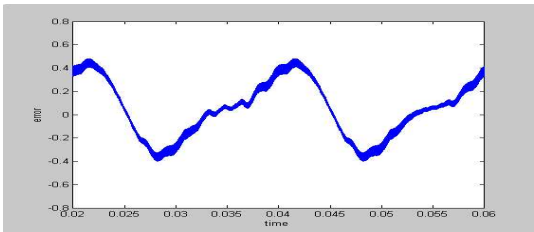

Figure 17: Voltage error using the equivalent control -with ZOH- as duty cycle (20kHz).

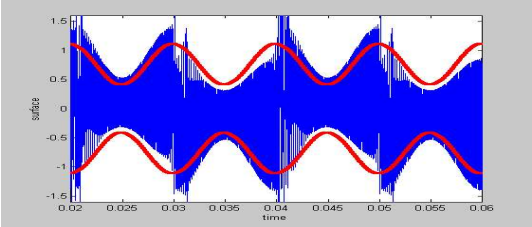

Figure 18: $S(x,t)$ using ZAD (10kHz).

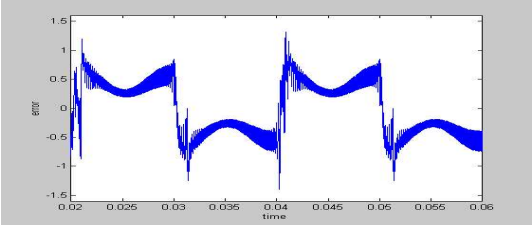

Figure 19: Voltage error using ZAD (10kHz).

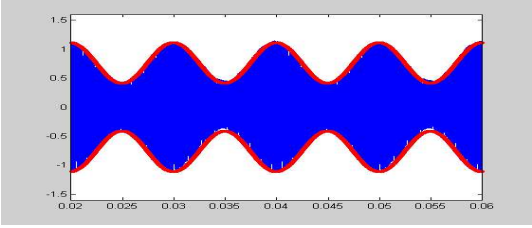

Figure 20: $S(x,t)$ using the equivalent control -without ZOH- as duty cycle (10kHz).

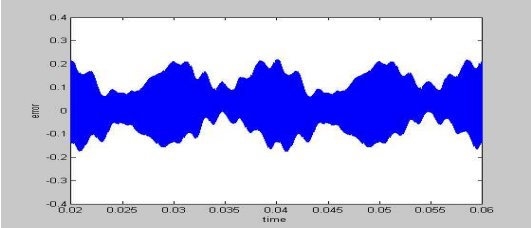

Figure 21: Voltage error using the equivalent control -without ZOH- as duty cycle (10kHz).

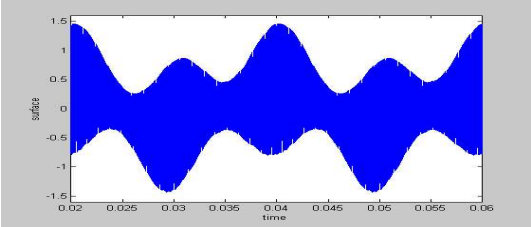

Figure 22: $S(x,t)$ using the equivalent control -with ZOH- as duty cycle (10kHz).

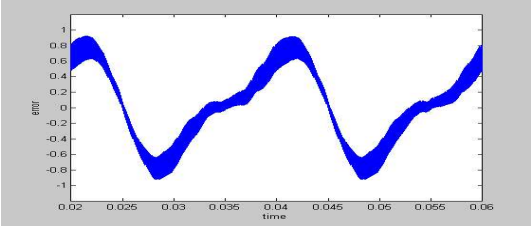

Figure 23: Voltage error using the equivalent control -with ZOH- as duty cycle (10kHz).

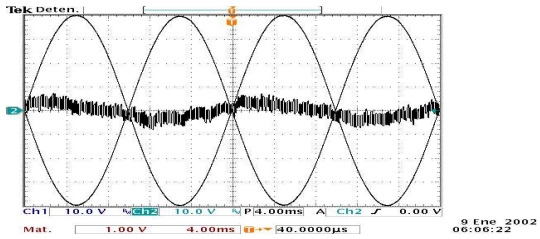

Figure 24: Output voltage, input signal (led 180^o) and voltage error in steady-state.

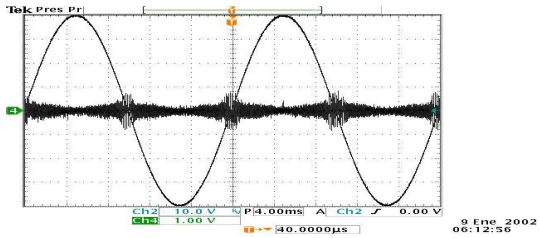

Figure 25: Output voltage and switching surface in steady-state.

the controller solves in real time.

The controller estimates the sliding surface derivatives, needed for solving the ZAD control algorithm, from sampling the switching surface at the beginning, the half and the end of the switching period. The duty cycle in the present switching period is solved from the estimate derivatives of the switching surface $S(x,t)$ and its value in the preceding switching period.

The steady-state dynamics of the output voltage, the voltage error signal and the switching surface are depicted in Figures 24 and 25. Figure 26 shows the transient dynamics when the load varies from open circuit to $R = 20\Omega$. As can be seen in this plot the ZAD control strategy maintains the robustness, which is the main sliding control mode characteristics.

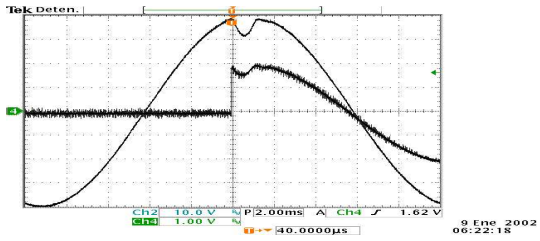

Figure 26: Performance of the output voltage and current when the load resistance varies.

3 SSA and GSSA for port controlled hamiltonian systems

3.1 Introduction

In this Section we describe a method, used mainly in the power converter literature, and known as GSSA (Generalized State Space Averaging), Selective Frequency Averaging or Multi-Frequency Averaging, which tries to extract a smooth system from a VSS. As an introduction, we present the SSA (State Space Averaging) approximation, which much better known in the literature and which can be considered as a particular case of GSSA. General references for GSSA, as applied to power converters, are [3], [12] and [18].

We apply the SSA and (truncated) GSSA approximations to a port hamiltonian model describing in a unified way all the second order power converters. The general relationship between the hamiltonian description of the approximations and the original hamiltonian description presented later in 3.6 is illustrated in this particular case.

From a more theoretical point of view, we give a short summary of [22], where some rigorous bounds on the convergence of the GSSA approximation are obtained. As stated above, in 3.6 we start with a general quadratic+linear hamiltonian and prove that its GSSA approximations are also hamiltonian. We give explicit expressions for the GSSA hamiltonian, structure and output functions, and apply the results to a full-bridge rectifier converter.

3.2 The SSA approximation

Assume a VSS system such that the change in the state variables is small over the time length of an structure change, or such that one is not interested about the fine details of the variation. Then one may try to formulate a dynamical system for the time average of the state variables

$$\langle x\rangle(t) = \frac{1}{T}\int_{t-T}^{t} x(\tau)\ \mathrm{d}\tau, \tag{42}$$

where T is the period, assumed constant, of a cycle of structure variations.

Let our VSS system be described in explicit port hamiltonian form

$$\dot{x} = \left[\mathcal{J}(S,x) - \mathcal{R}(S,x)\right](\nabla H(x))^T + g(S,x)u, \tag{43}$$

where S is a (multi)-index, with values on a finite, discrete set, enumerating the different structure topologies. For notational simplicity, we will assume from now on that we have a single index (corresponding to a single switch, or a set of switches with a single degree of freedom) and that $S \in \{0,1\}$. Hence, we have two possible dynamics, which we denote as

$$\begin{aligned} S=0 \quad &\Rightarrow \quad \dot{x} = (\mathcal{J}_0(x) - \mathcal{R}_0(x))(\nabla H(x))^T + g_0(x)u, \\ S=1 \quad &\Rightarrow \quad \dot{x} = (\mathcal{J}_1(x) - \mathcal{R}_1(x))(\nabla H(x))^T + g_1(x)u. \end{aligned} \tag{44}$$

Note that controlling the system means choosing the value of S as a function of the state variables, and that u is, in most cases, just a constant external input.

From (42) we have

$$\frac{\mathrm{d}}{\mathrm{d}t}\langle x\rangle(t) = \frac{x(t) - x(t-T)}{T}. \tag{45}$$

Now the central assumption of the SSA approximation method is that for a given structure we can substitute $x(t)$ by $\langle x\rangle(t)$ in the right-hand side of the dynamical equations, so that (44) become

$$\begin{aligned} S=0 \quad &\Rightarrow \quad \dot{x} \approx (\mathcal{J}_0(\langle x\rangle) - \mathcal{R}_0(\langle x\rangle))(\nabla H(\langle x\rangle))^T + g_0(\langle x\rangle)u, \\ S=1 \quad &\Rightarrow \quad \dot{x} \approx (\mathcal{J}_1(\langle x\rangle) - \mathcal{R}_1(\langle x\rangle))(\nabla H(\langle x\rangle))^T + g_1(\langle x\rangle)u. \end{aligned} \tag{46}$$

The rationale behind this approximation is that $\langle x\rangle$ does not have time to change too much during a cycle of structure changes. We assume also that the length of time in a given cycle when the system is in a given topology is determined by a function of the state variables or, in our approximation, a function of the averages, $t_0(\langle x\rangle)$, $t_1(\langle x\rangle)$, with $t_0 + t_1 = T$. Since we are considering the right-hand sides in (46) constant over the time scale of T, we can integrate the equations to get[2]

$$\begin{aligned} x(t) = x(t-T) \quad &+ \quad t_0(\langle x\rangle)\left[(\mathcal{J}_0(\langle x\rangle) - \mathcal{R}_0(\langle x\rangle))(\nabla H(\langle x\rangle))^T + g_0(\langle x\rangle)u\right] \\ &+ \quad t_1(\langle x\rangle)\left[(\mathcal{J}_1(\langle x\rangle) - \mathcal{R}_1(\langle x\rangle))(\nabla H(\langle x\rangle))^T + g_1(\langle x\rangle)u\right]. \end{aligned}$$

[2]We also assume that u does not vary over this time scale; in fact u is constant in many applications.

$S(x(t_k),t_k) \geq 0$ and $S(x(t_k),t_k) + \frac{T}{2}\dot{S}\Big\vert_{(k,u^+)} \geq 0$	$u(t_k) = u^+;\ d_k = 1$
$S(x(t_k),t_k) \geq 0$ and $S(x(t_k),t_k) + \frac{T}{2}\dot{S}\Big\vert_{(k,u^+)} < 0$	$u(t_k) = u^+;\ d_k = 1 - \sqrt{\frac{\vert\dot{S}\vert_{(k,u^+)}\vert - 2\frac{\vert S(x(t_k),t_k)\vert}{T}}{\vert\dot{S}\vert_{(k,u^+)}\vert + \vert\dot{S}\vert_{(k,u^-)}\vert}}$
$S(x(t_k),t_k) \leq 0$ and $S(x(t_k),t_k) + \frac{T}{2}\dot{S}\Big\vert_{(k,u^-)} \leq 0$	$u(t_k) = u^-;\ d_k = 1$
$S(x(t_k),t_k) \leq 0$ and $S(x(t_k),t_k) + \frac{T}{2}\dot{S}\Big\vert_{(k,u^+)} > 0$	$u(t_k) = u^-;\ d_k = 1 - \sqrt{\frac{\vert\dot{S}\vert_{(k,u^-)}\vert - 2\frac{\vert S(x(t_k),t_k)\vert}{T}}{\vert\dot{S}\vert_{(k,u^+)}\vert + \vert\dot{S}\vert_{(k,u^-)}\vert}}$

Table 1: ZAD control algorithm.

Using (45) we get the SSA equations for the variable $\langle x\rangle$:

$$\begin{aligned}\frac{\mathrm{d}}{\mathrm{d}t}\langle x\rangle &= d_0(\langle x\rangle)\left[(\mathcal{J}_0(\langle x\rangle)-\mathcal{R}_0(\langle x\rangle))(\nabla H(\langle x\rangle))^T+g_0(\langle x\rangle)u\right]\\ &+ d_1(\langle x\rangle)\left[(\mathcal{J}_1(\langle x\rangle)-\mathcal{R}_1(\langle x\rangle))(\nabla H(\langle x\rangle))^T+g_1(\langle x\rangle)u\right],\end{aligned} \tag{47}$$

where

$$d_{0,1}(\langle x\rangle)=\frac{t_{0,1}(\langle x\rangle)}{T}, \tag{48}$$

with $d_0+d_1=1$. In the power converter literature d_1 (or d_0, depending on the switch configuration) is referred to as the duty cycle.

3.3 The GSSA approximation

One can expect the SSA approximation to give poor results, as compared with the exact VSS model, for cases where T is not small with respect to the time scale of the changes of the state variables that we want to take into account. The GSSA approximation tries to solve this, and capture the fine detail of the state evolution, by considering a full Fourier series, and eventually truncating it, instead of just the "dc" term which appears in (42). Thus, one defines

$$\langle x\rangle_k(t)=\frac{1}{T}\int_{t-T}^{t}x(\tau)e^{-jk\omega\tau}\,\mathrm{d}\tau, \tag{49}$$

with $\omega=2\pi/T$ and $k\in\mathbb{Z}$. The time functions $\langle x\rangle_k$ are known as index-k averages or k-phasors. Notice that $\langle x\rangle_0$ is just $\langle x\rangle$.

Under standard assumptions about $x(t)$, one gets, for $\tau\in[t-T,t]$ with t fixed,

$$x(\tau)=\sum_{k=-\infty}^{+\infty}\langle x\rangle_k(t)e^{jk\omega\tau}. \tag{50}$$

If the $\langle x\rangle_k(t)$ are computed with (49) for a given t, then (50) just reproduces $x(\tau)$ periodically outside $[t-T,t]$, so it does not yield x outside of $[t-T,t]$ if x is not T-periodic. However, the idea of GSSA is to let t vary in (49) so that we really have a kind of "moving" Fourier series:

$$x(\tau)=\sum_{k=-\infty}^{+\infty}\langle x\rangle_k(t)e^{jk\omega\tau},\quad\forall\tau. \tag{51}$$

A more mathematically advanced discussion is presented in [22] and summarized in 3.5.

In order to obtain a dynamical GSSA model we need the following two essential properties:

- **Derivation.** Writing (49) as

$$\langle x\rangle_k(t)=\frac{1}{T}\int_{0}^{T}x(\tau+t-T)e^{-jk\omega(\tau+t-T)}\,\mathrm{d}\tau, \tag{52}$$

  one immediately gets

$$\frac{\mathrm{d}}{\mathrm{d}t}\langle x\rangle_k(t)=\left\langle\frac{\mathrm{d}x}{\mathrm{d}t}\right\rangle_k(t)-jk\omega\langle x\rangle_k(t). \tag{53}$$

- **Convolution.** If x and y are two signals, then

$$\langle xy\rangle_k=\sum_{l=-\infty}^{+\infty}\langle x\rangle_{k-l}\langle y\rangle_l. \tag{54}$$

  In particular, considering a first-harmonic GSSA approximation, one gets

$$\begin{aligned}\langle xy\rangle_0 &= \langle x\rangle_0\langle y\rangle_0+\langle x\rangle_{-1}\langle y\rangle_1+\langle x\rangle_1\langle y\rangle_{-1},\\ \langle xy\rangle_1 &= \langle x\rangle_0\langle y\rangle_1+\langle x\rangle_1\langle y\rangle_0,\\ \langle xy\rangle_{-1} &= \langle x\rangle_0\langle y\rangle_{-1}+\langle x\rangle_{-1}\langle y\rangle_0.\end{aligned} \tag{55}$$

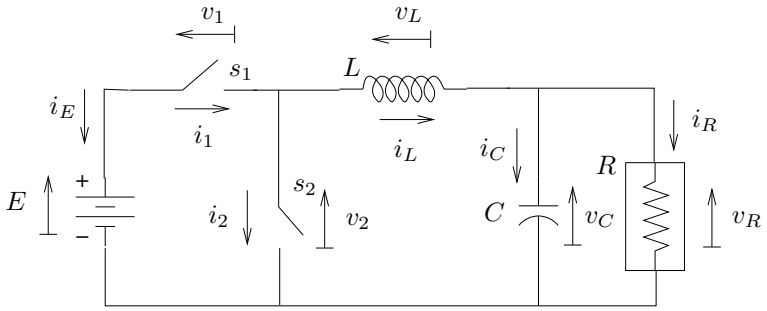

Figure 27: The buck converter.

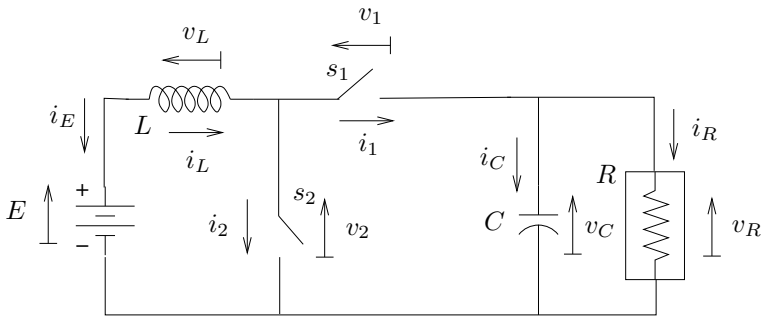

Figure 28: The boost converter.

Using (53) and (43) one gets

$$\begin{aligned}\frac{\mathrm{d}}{\mathrm{d}t}\langle x\rangle_k &= \left\langle \frac{\mathrm{d}x}{\mathrm{d}t}\right\rangle_k - jk\omega\langle x\rangle_k \\ &= \left\langle [\mathcal{J}(S,x)-\mathcal{R}(S,x)]\left(\nabla H(x)\right)^T + g(S,x)u\right\rangle_k - jk\omega\langle x\rangle_k. \end{aligned} \tag{56}$$

Assuming that the structure matrices $\mathcal{J}$ and $\mathcal{R}$, the hamiltonian H, and the interconnection matrix g have a series expansion in their variables, the convolution formula (54) can be used and an (infinite) dimensional system for the $\langle x\rangle_k$ can be obtained. More details for a general quadratic hamiltonian are presented in 3.6. Notice that, if we restrict ourselves to the dc terms (and without taking into consideration the contributions of the higher order harmonics to the dc averages), then (56) boils down to (47) since, under these assumptions, the zero-order average of a product is the product of the zero-order averages.

3.4 SSA and GSSA for second order power converters

Figures 27, 28, and 29 show the functional schemes of the buck, boost and buck-boost dc-dc power converters, respectively.

The VSS port hamiltonian models with the resistive port left open can be written in an unified way as

$$\dot{x} = \begin{pmatrix} 0 & \alpha-\beta S \\ -(\alpha-\beta S) & 0 \end{pmatrix}\left(\nabla H(x)\right)^T + \begin{pmatrix} -1 & 0 \\ 0 & 1-\gamma S \end{pmatrix}\begin{pmatrix} i_R \\ E \end{pmatrix}, \tag{57}$$

where the state variables are $x = (q_C \quad \phi_L)^T$ and the hamiltonian function is

$$H(q_c,\phi_L) = \frac{1}{2C}q_C^2 + \frac{1}{2L}\phi_L^2, \tag{58}$$

with $i_L = \partial_{\phi_L} H$, $v_C = \partial_{q_C} H$. The parameters corresponding to the different converters are given in Table 2. The variable $S = 0, 1$ represents the state of switch 2 (0 closed and 1 open), and switch 1 is

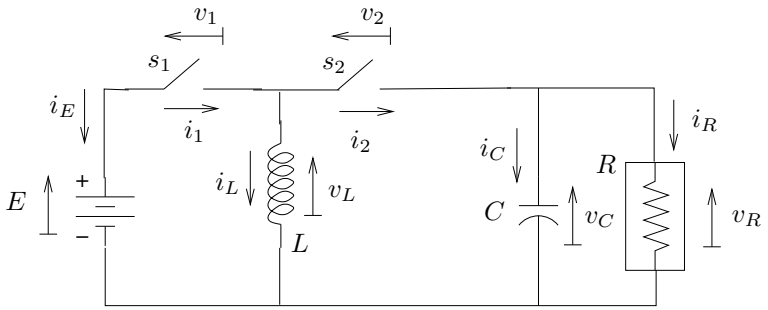

Figure 29: The buck-boost converter.

Converter	α	β	γ
buck	1	0	1
boost	1	1	0
buck-boost	0	1	1

Table 2: Parameter values for the unified description of the second-order power converters.

complementary to switch 2. The natural hamiltonian outputs of the system are

$$y = \begin{pmatrix} -1 & 0 \\ 0 & 1-\gamma S \end{pmatrix}^T (\nabla H(x))^T = \begin{pmatrix} -v_C \\ (1-\gamma S) i_L \end{pmatrix} = \begin{pmatrix} -v_R \\ -(1-\gamma S) i_E \end{pmatrix}. \tag{59}$$

The resistive port can be terminated (*i.e.* one can use $v_R = R i_R$) and then the structure matrix in (57) gets a dissipative part:

$$\dot{x} = \begin{pmatrix} -1/R & \alpha - \beta S \\ -(\alpha - \beta S) & 0 \end{pmatrix} (\nabla H(x))^T + \begin{pmatrix} 0 \\ 1-\gamma S \end{pmatrix} E. \tag{60}$$

Applying (47) to (60), one immediately gets

$$\begin{aligned} \frac{\mathrm{d}}{\mathrm{d}t}\langle x \rangle &= d_0(\langle x \rangle) \left[\begin{pmatrix} -1/R & \alpha \\ -\alpha & 0 \end{pmatrix} (\nabla H(\langle x \rangle))^T + \begin{pmatrix} 0 \\ 1 \end{pmatrix} E \right] \\ &+ d_1(\langle x \rangle) \left[\begin{pmatrix} -1/R & \alpha - \beta \\ -(\alpha - \beta) & 0 \end{pmatrix} (\nabla H(\langle x \rangle))^T + \begin{pmatrix} 0 \\ 1-\gamma \end{pmatrix} E \right] \\ &= \begin{pmatrix} -1/R & \alpha - \beta d_1(\langle x \rangle) \\ -(\alpha - \beta d_1(\langle x \rangle)) & 0 \end{pmatrix} (\nabla H(\langle x \rangle))^T + \begin{pmatrix} 0 \\ 1 - \gamma d_1(\langle x \rangle) \end{pmatrix} E, \end{aligned} \tag{61}$$

where $d_0 + d_1 = 1$ has been used. Since

$$\langle S \rangle = 0 \cdot d_0 + 1 \cdot d_1,$$

one finally gets

$$\frac{\mathrm{d}}{\mathrm{d}t}\langle x \rangle = \begin{pmatrix} -1/R & \alpha - \beta \langle S \rangle \\ -(\alpha - \beta \langle S \rangle) & 0 \end{pmatrix} (\nabla H(\langle x \rangle))^T + \begin{pmatrix} 0 \\ 1 - \gamma \langle S \rangle \end{pmatrix} E, \tag{62}$$

which is well-known in the literature in terms of co-energy variables.

Let us turn now to a GSSA truncated approximation, considering the fundamental terms and the first harmonics. Using the hamiltonian (58), we have

$$\frac{\mathrm{d}}{\mathrm{d}t} \begin{pmatrix} q_C \\ \phi_L \end{pmatrix} = \begin{pmatrix} -1/R & \alpha - \beta S \\ -(\alpha - \beta S) & 0 \end{pmatrix} \begin{pmatrix} \frac{q_C}{C} \\ \frac{\phi_L}{L} \end{pmatrix} + \begin{pmatrix} 0 \\ 1 - \gamma S \end{pmatrix}. \tag{63}$$

We define real variables x_i, $i = 1, \ldots, 6$ by means of

$$\begin{aligned}
\langle \phi_L \rangle_1 &= x_1 + j x_2, \\
\langle \phi_L \rangle_{-1} &= x_1 - j x_2, \\
\langle q_C \rangle_1 &= x_3 + j x_4, \\
\langle q_C \rangle_{-1} &= x_3 - j x_4, \\
\langle \phi_L \rangle_0 &= x_5, \\
\langle q_C \rangle_0 &= x_6,
\end{aligned}$$

so that, using (53),

$$\begin{aligned}
\dot{x}_1 &= \omega x_2 + \frac{1}{2}\left(\langle \dot{\phi}_L \rangle_1 + \langle \dot{\phi}_L \rangle_{-1} \right), \\
\dot{x}_2 &= -\omega x_1 + \frac{1}{2j}\left(\langle \dot{\phi}_L \rangle_1 - \langle \dot{\phi}_L \rangle_{-1} \right), \\
\dot{x}_3 &= \omega x_4 + \frac{1}{2}\left(\langle \dot{q}_C \rangle_1 + \langle \dot{q}_C \rangle_{-1} \right), \\
\dot{x}_4 &= -\omega x_3 + \frac{1}{2j}\left(\langle \dot{q}_C \rangle_1 - \langle \dot{q}_C \rangle_{-1} \right), \\
\dot{x}_5 &= \langle \dot{\phi}_L \rangle_0, \\
\dot{x}_6 &= \langle \dot{q}_C \rangle_0.
\end{aligned} \tag{64}$$

Next we compute the right-hand sides of (64) using (63) and the convolution property, and get

$$\begin{aligned}
\dot{x}_1 &= \omega x_2 - (\alpha - \beta \langle S \rangle_0) \frac{x_3}{C} + \beta \langle S \rangle_{1R} \frac{x_6}{C} - \gamma E \langle S \rangle_{1R}, \\
\dot{x}_2 &= -\omega x_1 - (\alpha - \beta \langle S \rangle_0) \frac{x_4}{C} + \beta \langle S \rangle_{1I} \frac{x_6}{C} - \gamma E \langle S \rangle_{1I}, \\
\dot{x}_3 &= (\alpha - \beta \langle S \rangle_0) \frac{x_1}{L} - \frac{1}{R}\frac{x_3}{C} + \omega x_4 - \beta \langle S \rangle_{1R} \frac{x_5}{L}, \\
\dot{x}_4 &= (\alpha - \beta \langle S \rangle_0) \frac{x_2}{L} - \omega x_3 - \frac{1}{R}\frac{x_4}{C} - \beta \langle S \rangle_{1I} \frac{x_5}{L}, \\
\dot{x}_5 &= 2\beta \langle S \rangle_{1R} \frac{x_3}{C} + 2\beta \langle S \rangle_{1I} \frac{x_4}{C} - (\alpha - \beta \langle S \rangle_0) \frac{x_6}{C} + E(1 - \gamma \langle S \rangle_0), \\
\dot{x}_6 &= -2\beta \langle S \rangle_{1R} \frac{x_1}{L} - 2\beta \langle S \rangle_{1I} \frac{x_2}{L} + (\alpha - \beta \langle S \rangle_0) \frac{x_5}{L} - \frac{1}{R}\frac{x_6}{C},
\end{aligned}$$

where $\langle S \rangle_{1R,1I}$ are the real and imaginary parts of $\langle S \rangle_1$. As it is shown in 3.6, using the hamiltonian

$$H_{PH} = \frac{1}{2L}(x_1^2 + x_2^2 + \frac{1}{2}x_5^2) + \frac{1}{2C}(x_3^2 + x_4^2 + \frac{1}{2}x_6^2), \tag{65}$$

this can be cast into hamiltonian form

$$\dot{x} = (\mathcal{J}_{PH} - \mathcal{R}_{PH})(\nabla H_{PH}(x))^T + g_{PH} E$$

with

$$\mathcal{J}_{PH} = \begin{pmatrix}
0 & \omega L & -\alpha + \beta \langle S \rangle_0 & 0 & 0 & 2\beta \langle S \rangle_{1R} \\
-\omega L & 0 & 0 & -\alpha + \beta \langle S \rangle_0 & 0 & 2\beta \langle S \rangle_{1I} \\
\alpha - \beta \langle S \rangle_0 & 0 & 0 & \omega C & -2\beta \langle S \rangle 1R & 0 \\
0 & \alpha - \beta \langle S \rangle_0 & -\omega C & 0 & -2\beta \langle S \rangle_{1I} & 0 \\
0 & 0 & 2\beta \langle S \rangle_{1R} & 2\beta \langle S \rangle_{1I} & 0 & -2(\alpha - \beta \langle S \rangle_0) \\
-2\beta \langle S \rangle_{1R} & -2\beta \langle S \rangle_{1I} & 0 & 0 & 2(\alpha - \beta \langle S \rangle_0) & 0
\end{pmatrix}, \tag{66}$$

$$\mathcal{R}_{PH} = \mathrm{diag}\left(0, 0, \frac{1}{R}, \frac{1}{R}, 0, \frac{2}{R}\right), \tag{67}$$

and

$$g_{PH} = \begin{pmatrix} -\gamma\langle S\rangle_{1R} \\ -\gamma\langle S\rangle_{1I} \\ 0 \\ 0 \\ 1-\gamma\langle S\rangle_0 \\ 0 \end{pmatrix} \tag{68}$$

3.5 Mathematical foundations of the GSSA method

In [22], Tadmor studies the case of dissipative systems with quadratically nonlinear lossless dynamics and gives some arguments to substantiate the approximation procedure for periodic solutions. More precisely, the type of systems considered there are described by an equation of the form

$$W\frac{d}{dt}x = -(D+S(x))x + f\,, \tag{69}$$

where $W > 0$, $D \geq 0$ and $S(x) = -S(x)^T$. The stored energy is $V(x) = \frac{1}{2}x^T W x$ and f is thought to be a periodic forcing term in some finite-dimensional space of Fourier coefficients $f \in \mathcal{F}(k_0)$. Two main situations are considered. One in which *transients* do not occur, and another one in which an abrupt deviation from steady-state might happen at some time —such as an impulsive disturbance or a change from one periodic forcing term to another.

We collect in what follows some of the results that are presented in [22]:

(i) The proof of existence of periodic solutions of system (69) is given and therefore of the corresponding harmonic balancing equations:

$$0 = -(D + jk\omega_0 W)\langle x\rangle_k(t) - \langle S(x)x\rangle_k(t) + \langle f\rangle_k(t)\,, \qquad k \in \mathbb{Z} \tag{70}$$

As a consequence, bounds on the phasors of exact, periodic solutions x are provided by

$$\|\langle x\rangle_k(t)\| \leq \frac{1}{\sqrt{k^2\omega_0^2+\lambda^2}} \cdot \begin{cases} (\|W^{-1}f\|_1 + \beta\rho^2)\,, & |k| \leq k_0 \\ \beta\rho^2\,, & |k| > k_0 \end{cases} \tag{71}$$

where the Euclidean norm is used and λ, β, ρ are constants depending on the data of the system and a neighborhood of the periodic solution. Moreover, it is shown how these bounds for $k > k_0$ can be replaced by higher-order decay bounds of the form

$$\|\langle x\rangle_k(t)\| \leq \frac{\nu_l}{k^l}\|x\|_2 \leq \frac{\mu_l}{k_l} \tag{72}$$

where again, ν_l and μ_l are adequate constants. These bounds provide absolute and relative error bounds when truncating the Fourier series of the periodic solutions.

(ii) The paper follows along the same lines to prove the existence of periodic solutions $\tilde{x}$ of the *compressed balancing equations*. That is, the set of the first l equations of (70). Similar bounds to the former ones are obtained for these *compressed* solutions $\tilde{x}$ in terms of the Euclidean and L_∞ norms.

(iii) Then, under some technical conditions that include a regularity assumption for the operator

$$\Lambda_l(\phi) = W\frac{d}{d\tau}\phi + D\phi + \Pi_l(S(\phi)\phi)\,,$$

defined on $\Lambda_l : \mathcal{F}(l) \longrightarrow \mathcal{F}(l)$, a first approximation result is given that, roughly speaking, states how an approximate periodic solution $\tilde{x}$ becomes increasingly close to an exact periodic solution x.

(iv) The last part of the paper deals with the same type of approximations but when transients are also considered. Given an initial state history x_{t_0}, it is assumed that after a transient the corresponding solution with settle at a stable steady state ϕ. It is observed that, unlike what happens in the non-transient case, here there are not bounds available for phasor decay rates of compressed solutions, and for exact solutions these bounds only yield the first order decay rate (71) while the Fourier expansion does not converge uniformly on $[T-t, t]$. Now the main result states that for a sufficiently large l the $\mathcal{F}(l)$ compression of the dynamic phasor model, gives rise to a good approximation of x during transients and will converge to a neighborhood of $\Pi_l\phi$. The approximation can only be provided in terms of L_2 norms.

(v) Finally, some numerical examples are presented in which the strengths and weaknesses of the theory are shown. In particular, the numerical simulations show a better performance when the truncated Fourier series are evaluated with a half-period delay. This is previously supported by the following fact. A signal can be expressed as the sum of $x = x_p + x_{lin}$, where x_p is a periodic signal and x_{lin} is the straight line passing through $x_{lin}(t - \frac{T}{2}) = 0$ with a slope of $\frac{1}{T}(x(t) - x(t-T))$. It can be seen that the Fourier expansion of x_{lin} converges uniformly over any open set of $[t-T, t]$, that symmetric tails of its expansion are uniformly bounded on the entire $[t-T, t]$ that its symmetric subseries actually vanish at the middle point $t - \frac{T}{2}$. This could explain the better performance of algorithms when mid-point evaluations are taken.

3.6 GSSA for quadratic hamiltonians

Consider a port-controlled Hamiltonian system defined by

$$\dot{z} = (J(z,v) - R(z))\,\frac{\partial H}{\partial z} + f\,, \qquad z \in \mathbb{R}^n \tag{73}$$

with a Hamiltonian function of the form

$$H = \frac{1}{2} z^T W z + D^T z\,, \qquad W > 0\,, \text{ and } W^T = W\,.$$

This Hamiltonian satisfies $\dfrac{\partial H}{\partial z} = Wz + D$ and

$$\langle \frac{\partial H}{\partial z} \rangle_l = W\langle z\rangle_l + \langle D\rangle_l = \begin{cases} W\langle z\rangle_0 + D\,, & l = 0 \\ W\langle z\rangle_l\,, & l \neq 0 \end{cases}$$

and, therefore, the phasor system associated with (73) is given by

$$\begin{aligned} \frac{d}{dt}\langle z\rangle_k &= -jkw_0\langle z\rangle_k + \langle (J-R)\frac{\partial H}{\partial z}\rangle_k + \langle f\rangle_k \\ &= -jkw_0\langle z\rangle_k + (\langle J\rangle_k - \langle R\rangle_k)(W\langle z\rangle_0 + D) + \sum_{l=-\infty,\, l\neq 0}^{+\infty} (\langle J\rangle_{k-l} - \langle R\rangle_{k-l})\cdot W\langle z\rangle_l + \langle f\rangle_k. \end{aligned}$$

In this derivation we have made use of $\dfrac{d}{dt}\langle z\rangle_k = \langle \dot{z}\rangle_k - jk\omega_0\langle z\rangle_k$ and the set of formal equalities

$$\begin{aligned} \langle J\cdot Wz\rangle_k &= \left(\sum_j \langle J_{ij}(Wz)^j\rangle_k\right)_{1\le i\le n} = \left(\sum_j \sum_{l=-\infty}^{\infty} \langle J_{ij}\rangle_{k-l}\langle (Wz)^j\rangle_l\right)_{1\le i\le n} \\ &= \left(\sum_{l=-\infty}^{\infty}\sum_j \langle J_{ij}\rangle_{k-l}\langle (Wz)^j\rangle_l\right)_{1\le i\le n} = \sum_{l=-\infty}^{+\infty}\langle J\rangle_{k-l}\langle Wz\rangle_l = \sum_{l=-\infty}^{+\infty}\langle J\rangle_{k-l}\cdot W\langle z\rangle_l\,. \end{aligned}$$

To better identify the Hamiltonian structure of the phasor equations, we will split them into their real and imaginary parts:

$$\begin{aligned} \frac{d}{dt}\langle z\rangle_k^R &= k\omega_0\langle z\rangle_k^I + (\langle J\rangle_k^R - \langle R\rangle_k^R)(W\langle z\rangle_0 + D) \\ &\quad + \sum_{l=-\infty,\, l\neq 0}^{+\infty} \left[(\langle J\rangle_{k-l}^R - \langle R\rangle_{k-l}^R)W\langle z\rangle_l^R - (\langle J\rangle_{k-l}^I - \langle R\rangle_{k-l}^I)W\langle z\rangle_l^I\right] + \langle f\rangle_k^R\,, \\ \frac{d}{dt}\langle z\rangle_k^I &= -k\omega_0\langle z\rangle_k^R + (\langle J\rangle_k^I - \langle R\rangle_k^I)(W\langle z\rangle_0 + D) \\ &\quad + \sum_{l=-\infty,\, l\neq 0}^{+\infty} \left[(\langle J\rangle_{k-l}^I - \langle R\rangle_{k-l}^I)W\langle z\rangle_l^R + (\langle J\rangle_{k-l}^R - \langle R\rangle_{k-l}^R)W\langle z\rangle_l^I\right] + \langle f\rangle_k^I\,. \end{aligned}$$

Or, equivalently, using that $\langle z\rangle_{-l} = \overline{\langle z\rangle_l}$ and gathering the coefficients of $W\langle z\rangle_l^R$ and $W\langle z\rangle_l^I$, $\forall l \in \mathbb{Z}$, these equations can be expressed as

$$\frac{d}{dt}\langle z\rangle_0 = (\langle J\rangle_0 - \langle R\rangle_0)\,(W\langle z\rangle_0 + D) + 2\sum_{l=1}^{\infty}\left[\left(\langle J\rangle_l^R - \langle R\rangle_l^R\right)W\langle z\rangle_l^R + \left(\langle J\rangle_l^I - \langle R\rangle_l^I\right)W\langle z\rangle_l^I\right] + \langle f\rangle_0\,, \quad (74)$$

$$\frac{d}{dt}\langle z\rangle_k^R = k\omega_0\langle z\rangle_k^I + (\langle J\rangle_k^R - \langle R\rangle_k^R)(W\langle z\rangle_0 + D) + \sum_{l=1}^{+\infty}\left[\left(\langle J\rangle_{k-l}^R - \langle R\rangle_{k-l}^R + \langle J\rangle_{k+l}^R - \langle R\rangle_{k+l}^R\right)W\langle z\rangle_l^R - \left(\langle J\rangle_{k-l}^I - \langle R\rangle_{k-l}^I - \langle J\rangle_{k+l}^I + \langle R\rangle_{k+l}^I\right)W\langle z\rangle_l^I\right] + \langle f\rangle_k^R\,, \quad (75)$$

$$\frac{d}{dt}\langle z\rangle_k^I = -k\omega_0\langle z\rangle_k^R + (\langle J\rangle_k^I - \langle R\rangle_k^I)(W\langle z\rangle_0 + D) + \sum_{l=1}^{+\infty}\left[\left(\langle J\rangle_{k-l}^I - \langle R\rangle_{k-l}^I + \langle J\rangle_{k+l}^I - \langle R\rangle_{k+l}^I\right)W\langle z\rangle_l^R + \left(\langle J\rangle_{k-l}^R - \langle R\rangle_{k-l}^R - \langle J\rangle_{k+l}^R + \langle R\rangle_{k+l}^R\right)W\langle z\rangle_l^I\right] + \langle f\rangle_k^I\,. \quad (76)$$

Consider now the Hamiltonian function defined by the formal series expansion

$$H_{\mathsf{PH}} = \frac{1}{2}D^T\langle z\rangle_0 + \frac{1}{4}\sum_{k=-\infty}^{\infty}\langle z\rangle_{-k}^T W\langle z\rangle_k = \frac{1}{2}D^T\langle z\rangle_0 + \frac{1}{4}\langle z\rangle_0^T W\langle z\rangle_0 + \frac{1}{2}\sum_{k=1}^{+\infty}(\langle z\rangle_k^{R,T}W\langle z\rangle_k^R + \langle z\rangle_k^{I,T}W\langle z\rangle_k^I)\,.$$

The main property of this Hamiltonian is that it satisfies

$$2\frac{\partial H_{\mathsf{PH}}}{\partial\langle z\rangle_0} = \langle\frac{\partial H}{\partial z}\rangle_0\,, \qquad \frac{\partial H_{\mathsf{PH}}}{\partial\langle z\rangle_k^R} = \langle\frac{\partial H}{\partial z}\rangle_k^R\,, \qquad \frac{\partial H_{\mathsf{PH}}}{\partial\langle z\rangle_k^I} = \langle\frac{\partial H}{\partial z}\rangle_k^I\,, \qquad \forall k \geq 1\,.$$

Then, equations (74)–(76), $k \in \mathbb{Z}$, can be rewritten as the infinite-dimensional Hamiltonian system

$$\Sigma_{\mathsf{PH}}: \quad \frac{d}{dt}\langle z\rangle = (J_{\mathsf{PH}} - R_{\mathsf{PH}})\frac{\partial H_{\mathsf{PH}}}{\partial\langle z\rangle} + f_{\mathsf{PH}}\,, \quad (77)$$

where $\langle z\rangle = (\langle z\rangle_0^T, \langle z\rangle_1^{R,T}, \langle z\rangle_1^{I,T}, \ldots, \langle z\rangle_k^{R,T}, \langle z\rangle_k^{I,T}, \ldots)^T$, J_{PH} (respectively R_{PH}) is a infinite-dimensional matrix, and $f_{\mathsf{PH}} = (\langle f\rangle_0^T, \langle f\rangle_1^{R,T}, \langle f\rangle_1^{I,T}, \ldots, \langle f\rangle_k^{R,T}, \langle f\rangle_k^{I,T}, \ldots)^T$.

Using that $\langle J\rangle_{-k} = \overline{\langle J\rangle_k}$, we can find the following expression for the first $k \times k$ block submatrix of J_{PH}:

$$\begin{pmatrix} 2\langle J\rangle_0\,, & 2\langle J\rangle_1^R\,, & 2\langle J\rangle_1^I\,, & \ldots & 2\langle J\rangle_k^R\,, & 2\langle J\rangle_k^I \\ 2\langle J\rangle_1^R\,, & \langle J\rangle_0 + \langle J\rangle_2^R\,, & \omega_0 W^{-1} + \langle J\rangle_2^I\,, & \ldots & \langle J2\rangle_{k-1}^R + \langle J\rangle_{k+1}^R\,, & \langle J\rangle_{k-1}^I + \langle J\rangle_{k+1}^I \\ 2\langle J\rangle_1^I\,, & -\omega_0 W^{-1} + \langle J\rangle_2^I\,, & \langle J\rangle_0 - \langle J\rangle_2^R\,, & \ldots & -\langle J2\rangle_{k-1}^I + \langle J\rangle_{k+1}^I\,, & \langle J\rangle_{k-1}^R - \langle J\rangle_{k+1}^R\,, \\ \ldots & \ldots & \ldots & \ldots & \ldots & \ldots \\ 2\langle J\rangle_k^R\,, & \langle J\rangle_{k-1}^R + \langle J\rangle_{k+1}^R\,, & -\langle J\rangle_{k-1}^I + \langle J\rangle_{k+1}^I\,, & \ldots & \langle J\rangle_0 + \langle J\rangle_{2k}^R\,, & k\omega_0 W^{-1} + \langle J\rangle_{2k}^I \\ 2\langle J\rangle_k^I\,, & \langle J\rangle_{k-1}^I + \langle J\rangle_{k+1}^I\,, & \langle J\rangle_{k-1}^R - \langle J\rangle_{k+1}^R\,, & \ldots & -k\omega_0 W^{-1} + \langle J\rangle_{2k}^I\,, & \langle J\rangle_0 - \langle J\rangle_{2k}^R \end{pmatrix}$$

Since $J^T + J = 0$, we have $\langle J^T + J\rangle_k = 0$. By definition $\langle J\rangle_k = (\langle J_{ij}\rangle_k)$ and then $\langle J\rangle_k^T = -\langle J\rangle_k$, $\forall k$. On the other hand, it is easy to see that

$$(-k\omega_0 W^{-1} + \langle J\rangle_{2k}^I)^T = -k\omega_0 W^{-1} - \langle J\rangle_{2k}^I = -(k\omega_0 W^{-1} + \langle J\rangle_{2k}^I)\,,\ \forall k \in \mathbb{N}\,.$$

All these facts can be used together to prove the antisymmetry of J_{PH} by induction on its $k \times k$ block submatrices.

The expression for a general $k \times k$ block submatrix of R_{PH} is similar to the above one and is given by

$$\begin{pmatrix} 2\langle R\rangle_0\,, & 2\langle R\rangle_1^R\,, & 2\langle R\rangle_1^I\,, & \dots & 2\langle R\rangle_k^R\,, & 2\langle R\rangle_k^I\,, \\ 2\langle R\rangle_1^R\,, & \langle R\rangle_0 + \langle R\rangle_2^R\,, & \langle R\rangle_2^I\,, & \dots & \langle R\rangle_{k-1}^R + \langle R2\rangle_{k+1}^R\,, & \langle R\rangle_{k-1}^I + \langle R\rangle_{k+1}^I \\ 2\langle R\rangle_1^I\,, & \langle R\rangle_2^I\,, & \langle R\rangle_0 - \langle R\rangle_2^R\,, & \dots & -\langle R\rangle_{k-1}^I + \langle R\rangle_{k+1}^I\,, & \langle R\rangle_{k-1}^R - \langle R\rangle_{k+1}^R\,, \\ \dots & \dots & \dots & \dots & \dots & \dots \\ 2\langle R\rangle_k^R\,, & \langle R\rangle_{k-1}^R + \langle R\rangle_{k+1}^R\,, & -\langle R\rangle_{k-1}^I + \langle R\rangle_{k+1}^I\,, & \dots & \langle R\rangle_0 + \langle R\rangle_{2k}^R\,, & \langle R\rangle_{2k}^I\,, \\ 2\langle R\rangle_k^I\,, & \langle R\rangle_{k-1}^I + \langle R\rangle_{k+1}^I\,, & \langle R\rangle_{k-1}^R - \langle R\rangle_{k+1}^R\,, & \dots & \langle R\rangle_{2k}^I\,, & \langle R\rangle_0 - \langle R\rangle_{2k}^R\,, \end{pmatrix}$$

Again, because of the symmetry of R, this submatrix is also symmetric and so will be R_{PH}.

Remark 3.1 For Hamiltonians H of the form

$$W = \begin{pmatrix} W_1 & 0 \\ 0 & 0 \end{pmatrix},$$

such that $W_1 > 0$, and $2H(z) = 2H(z_1, z_2) = z_1^T W_1 z_1$, we can also derive a phasor Hamiltonian system that differs from the previous one in the expressions for J_{PH} and f_{PH}. To define the new J_{PH} we only have to substitute

$$\begin{pmatrix} W_1^{-1} & 0 \\ 0 & 0 \end{pmatrix},$$

by W^{-1} in the former J_{PH}. Observe this does not spoil the antisymmetry of J_{PH} and it still accounts for the terms $k\omega_0\langle z_1\rangle_k^I$ and $-k\omega_0\langle z_1\rangle_k^R$. However, the other terms $k\omega_0\langle z_2\rangle_k^I$ and $-k\omega_0\langle z_2\rangle_k^R$ are necessarily to be included in f_{PH} as

$$f_{\mathsf{PH}} = \langle f\rangle + \left(0, 0, 0, \omega_0\langle z_2\rangle_1^{I,T}, 0, -\omega_0\langle z_2\rangle_1^{R,T}, 0, \dots, 0, k\omega_0\langle z_2\rangle_k^{I,T}, 0, -k\omega_0\langle z_2\rangle_k^{R,T}, 0, \dots\right)^T$$

An example of this situation is the following model of a full-bridge rectifier with a resistive load.

Example 3.2 (Full-bridge rectifier with a resistive load) The equations of a full-bridge rectifier [10] with a resistive load are given by

$$\begin{aligned} &\frac{dz}{dt} = (J(v) - R(z))\,\frac{\partial H}{\partial z} + f\,, \\ &\text{where } z = (z_1, z_2)^T = (\phi, \frac{1}{2}q^2)^T\,, \quad H = \frac{1}{2L}z_1^2 + \frac{1}{C}z_2\,, \quad f = (E\sin(\omega_0 t), 0)^T = (v_i, 0)^T \\ &\text{and } J = \begin{pmatrix} 0 & v \\ -v & 0 \end{pmatrix}, \quad R = \begin{pmatrix} r & 0 \\ 0 & \frac{2z_2}{R} \end{pmatrix}. \end{aligned}$$

In this particular case, the phasor Hamiltonian is

$$H_{\mathsf{PH}} = \frac{1}{2C}\langle z_2\rangle_0 + \frac{1}{4L}\langle z_1\rangle_0^2 + \frac{1}{2L}\sum_{k=1}^{\infty}\left(\langle z_1\rangle_k^{R^2} + \langle z_1\rangle_k^{I^2}\right),$$

the matrices J_{PH}, R_{PH} are

$$J_{\mathsf{PH}} = \begin{pmatrix} 0 & 2\langle v\rangle_0 & 0 & 2\langle v\rangle_1^R & 0 & 2\langle v\rangle_1^I & \dots \\ -2\langle v\rangle_0 & 0 & -2\langle v\rangle_1^R & 0 & -2\langle v\rangle_1^I & 0 & \dots \\ 0 & 2\langle v\rangle_1^R & 0 & \langle v\rangle_0 + \langle v\rangle_2^R & \omega_0 L & \langle v\rangle_2^I & \dots \\ -2\langle v\rangle_1^R & 0 & -\langle v\rangle_0 - \langle v\rangle_2^R & 0 & -\langle v\rangle_2^I & 0 & \dots \\ 0 & 2\langle v\rangle_1^I & -\omega_0 L & \langle v\rangle_2^I & 0 & \langle v\rangle_0 - \langle v\rangle_2^R & \dots \\ -2\langle v\rangle_1^I & 0 & -\langle v\rangle_2^I & 0 & -\langle v\rangle_0 + \langle v\rangle_2^R & 0 & \dots \\ \dots & \dots & \dots & \dots & \dots & \dots & \dots \end{pmatrix}$$

and

$$R_{\mathsf{PH}} = \begin{pmatrix} 2r & 0 & 0 & 0 & 0 & 0 & \dots \\ 0 & \frac{4\langle z_2\rangle_0}{R} & 0 & \frac{4\langle z_2\rangle_1^R}{R} & 0 & \frac{4\langle z_2\rangle_1^I}{R} & \dots \\ 0 & 0 & r & 0 & 0 & 0 & \dots \\ 0 & \frac{4\langle z_2\rangle_1^R}{R} & 0 & \frac{2}{R}\left(\langle z_2\rangle_0 + \langle z_2\rangle_2^R\right) & 0 & \frac{2\langle z_2\rangle_1^I}{R} & \dots \\ 0 & 0 & 0 & 0 & r & 0 & \dots \\ 0 & \frac{4\langle z_2\rangle_1^R}{R} & 0 & \frac{2\langle z_2\rangle_1^I}{R} & 0 & \frac{2}{R}\left(\langle z_2\rangle_0 - \langle z_2\rangle_2^R\right) & \dots \\ \dots & \dots & \dots & \dots & \dots & \dots & \dots \end{pmatrix},$$

and the expression of f_{PH} is given by

$$f_{\mathsf{PH}}^T = \left(0,\ 0,\ v_i,\ \omega_0\langle z_2\rangle_1^I,\ 0,\ -\omega_0\langle z_2\rangle_1^R,\ 0,\ \dots, 0,\ k\omega_0\langle z_2\rangle_k^I,\ 0,\ -k\omega_0\langle z_2\rangle_k^R,\ 0,\ \dots\right).$$

Now, it can be shown that the associated phasor system can be recovered as:

$$\frac{d}{dt}\langle z\rangle = (J_{\mathsf{PH}} - R_{\mathsf{PH}})\,\frac{\partial H_{\mathsf{PH}}}{\partial\langle z\rangle} + f_{\mathsf{PH}}\,.$$

3.6.1 Projection of Σ_{PH}

Consider that Σ_{PH} is a system defined on the infinite-dimensional space of Fourier coefficients $\mathcal{F}$ whose states are given by the tuples $(\langle z\rangle_0, \langle z\rangle_1^R, \langle z\rangle_1^I, \dots)$ such that $z(t+\tau) = \sum_{k=-\infty}^{+\infty}\langle z\rangle_k(t)\mathrm{e}^{jk\omega_0\tau}$ converges.

Le us define the finite-dimensional spaces $\mathcal{F}_{(k_1,\dots,k_s)}$ as those whose elements are of the form $(\langle z\rangle_{k_1}, \langle z\rangle_{k_2}, \dots, \langle z\rangle_{k_s})$, where k_i is implicitly a function of R or I (meaning that we take the real or imaginary part of phasor $\langle z\rangle_{k_i}$). We can define a projection from $\mathcal{F}$ to $\mathcal{F}_{(k_1,\dots,k_s)}$ which can be interpreted as a truncation of a series $\sum_{k=-\infty}^{+\infty}\langle z\rangle_k(t)\mathrm{e}^{jk\omega_0\tau}$ in $\mathcal{F}$ to the associated sum $\sum_{l=k_1}^{s}\langle z\rangle_l$ in $\mathcal{F}_{(k_1,\dots,k_s)}$. We call this projection $\pi_{(k_1,\dots,k_s)} : \mathcal{F} \longrightarrow \mathcal{F}_{(k_1,\dots,k_s)}$, and denote it by π when it is clear from the context which truncation we are referring to. Sometimes we will abuse of notation and consider $\mathcal{F}_{(k_1,\dots,k_s)}$ as a subspace of $\mathcal{F}$.

A natural question that arises now is whether the Hamiltonian structure of Σ_{PH} is preserved under these projections. The answer will be positive due to the following observation. If from a symmetric (respectively antisymmetric) matrix we delete the same numbered column and row (say, row i and column i), then the resulting matrix will preserve its symmetry (or its antisymmetry).

Applying a projection $\pi_{(k_1,\dots,k_s)} \equiv \pi$ to Σ_{PH} gives rise to a new system Σ_π in which the differential equations associated with $\langle z\rangle_l$, $l \neq k_i$ are not present. In terms of the associated matrices J_{PH} and R_{PH}, this means we have to remove all rows corresponding to $\langle z\rangle_l$ with $l \neq k_i$, $1 \leq i \leq s$ and set to zero any contribution of $\langle z\rangle_l$ in the other entries of J_{PH} and R_{PH}. On the other hand, since $\dfrac{\partial H_{\mathsf{PH}}}{\partial\langle z\rangle_l}$ depends linearly on $\langle z\rangle_l$, the contributions of the columns that are multiplied by $\dfrac{\partial H_{\mathsf{PH}}}{\partial\langle z\rangle_l}$ should not be considered either. In other words, for each $\langle z\rangle_l$ row, we should also ignore the same $W\langle z\rangle_l$ column of J_{PH} and R_{PH}. This operation defines new antisymmetric and symetric matrices, J_π and R_π, which together with H_π, obtained by setting to zero $\langle z\rangle_l$ in H_{PH}, define a new Hamiltonian system:

$$\Sigma_\pi : \quad \dot{x} = (J_\pi - R_\pi)\frac{\partial H_\pi}{\partial x} + f_\pi\,,$$

with $x = (\langle z\rangle_{k_1}, \langle z\rangle_{k_2}, \dots, \langle z\rangle_{k_s})$ and $f_\pi = (\langle f\rangle_{k_1}, \dots, \langle f\rangle_{k_s})$.

Remark 3.3 In case the original hamiltonian H was defined by a matrix

$$W = \begin{pmatrix} W_1 & 0 \\ 0 & W_2 \end{pmatrix}$$

we could also apply additional projections that respect the Hamiltonian structure of the phasors' system. These projections are induced by $\tau_1 : z \longmapsto z_1$ and $\tau_2 : z \longmapsto z_2$ such that $z^T W z = z_1^T W_1 z_1 + z_2^T W_2 z_2$ and $z = (z_1^T, z_2^T)^T$. Then, $\langle z\rangle_l = (\langle z_1\rangle_l^T, \langle z_2\rangle_l^T)^T$ and $\dfrac{\partial H_{\mathsf{PH}}}{\partial\langle z_1\rangle_l} = W_1\langle z_1\rangle_l$, $\dfrac{\partial H_{\mathsf{PH}}}{\partial\langle z_2\rangle_l} = W_2\langle z_2\rangle_l$. Again, this linearity allows us to say that for each $\langle z_1\rangle_l$ (respectively $\langle z_2\rangle_l$) row we delete in the phasors' system, we have to neglect the contribution of the $\langle z_1\rangle_l$ (respectively $\langle z_2\rangle_l$) column of J_{PH} and R_{PH} matrices. In this way, their antisymmetry or symmetry will be preserved.

3.6.2 Control of Σ_{PH} though Σ_π

Under some mild conditions the process described in the former subsection could help us control the original system Σ by controlling a projection Σ_π.

Suppose we want to design our system so that it follows a desired signal in steady state. Assume also that after an analysis of the equations of the system we find that the harmonic contents of the states and inputs in steady state are in $\mathcal{F}_{(k_1,\dots,k_l)}$, where f belongs too. Now, applying the projection $\pi_{(k_1,\dots,k_l)}$ to Σ_{PH} we obtain Σ_π that we design using PBC. That is, from

$$\Sigma_\pi : \quad \dot{x} = (J_\pi(x,u) - R_\pi(x))\frac{\partial H_\pi}{\partial x} + f$$

we define $u = \beta(x)$, $J_\pi^d(x) = J_\pi(x,\beta(x))$, $R_\pi^d(x) = R_\pi(x)$ and $H_\pi^d(x) = H_\pi(x) + H_a(x)$, so that the above system can be rewritten as

$$\Sigma_\pi^d : \quad \dot{x} = (J_\pi^d(x) - R_\pi^d(x))\frac{\partial H_\pi^d}{\partial x}\,.$$

From now on we will only consider projections π such that H_π includes the linear term $D^T\langle z\rangle_0$. Let us write with a slight abuse of notation $\langle z\rangle = (x, x_r)$ and $H_{\mathsf{PH}}(x,x_r) = H_\pi(x) + H_r(x_r)$. In fact,

$$\frac{\partial H_{\mathsf{PH}}}{\partial x} = \frac{\partial H_\pi}{\partial x}\,, \qquad \frac{\partial H_{\mathsf{PH}}}{\partial x_r} = \frac{\partial H_r}{\partial x_r}\,, \qquad \frac{\partial H_r}{\partial x} = \frac{\partial H_\pi}{\partial x_r} = 0\,.$$

The same holds if we take instead $H_{\mathsf{PH}}^d(x,x_r) = H_\pi^d(x) + H_r(x_r)$.

Consider the state $\langle z\rangle_* = (x_*, 0)$ or, in other words, $\pi\langle z\rangle_* = x_*$. Then,

$$\left(\frac{d}{dt}H_{\mathsf{PH}}^d\right)_{|\langle z\rangle_*} = \left(\frac{\partial H_{\mathsf{PH}}^d}{\partial\langle z\rangle}\cdot\frac{d}{dt}\langle z\rangle\right)_{|\langle z\rangle_*} = 0$$

because of

$$\frac{\partial H_{\mathsf{PH}}^d}{\partial\langle z\rangle}_{|\langle z\rangle_*} = \left(\frac{\partial H_{\mathsf{PH}}^d}{\partial x}_{|\langle z\rangle_*}, \frac{\partial H_{\mathsf{PH}}^d}{\partial x_r}_{|\langle z\rangle_*}\right) = \left(\frac{\partial H_\pi^d}{\partial x}_{|\langle z\rangle_*}, \frac{\partial H_r}{\partial x_r}_{|\langle z\rangle_*}\right) = (0,0)\,.$$

If we compute the derivative of H_{PH}^d along the trajectories of Σ_{PH} we obtain:

$$\begin{aligned}
\frac{d}{dt}H_{\mathsf{PH}}^d &= \left(\frac{\partial H_\pi^d}{\partial\langle z\rangle}\right)^T\cdot\frac{d\langle z\rangle}{dt} + \left(\frac{\partial H_r}{\partial\langle z\rangle}\right)^T\cdot\frac{d\langle z\rangle}{dt}\\
&= \left(\frac{\partial H_\pi^d}{\partial x}\right)^T\left(J_\pi^d - R_\pi^d\right)\frac{\partial H_\pi^d}{\partial x} + \left(\frac{\partial H_r}{\partial\langle z\rangle}\right)^T\cdot\frac{d\langle z\rangle}{dt}\\
&= -\left(\frac{\partial H_\pi^d}{\partial x}\right)^T R_\pi^d\frac{\partial H_\pi^d}{\partial x} + \left(\frac{\partial H_r}{\partial\langle z\rangle}\right)^T\left[\left(J_{\mathsf{PH}} - R_{\mathsf{PH}}\right)\frac{\partial H_{\mathsf{PH}}}{\partial\langle z\rangle} + f_{\mathsf{PH}}\right]
\end{aligned}$$

It is easy to see that for either $f_{\mathsf{PH}} \in \mathcal{F}_{(k_1,\dots,k_l)}$ or as Remark 3.1, $\left(\frac{\partial H_r}{\partial\langle z\rangle}\right)^T\cdot f_{\mathsf{PH}} = 0$ holds, and the former expression can further be developed as

$$\begin{aligned}
\frac{d}{dt}H_{\mathsf{PH}}^d &= -\left(\frac{\partial H_\pi^d}{\partial x}\right)^T R_\pi^d\frac{\partial H_\pi^d}{\partial x} + \left(\frac{\partial H_r}{\partial\langle z\rangle}\right)^T\left(J_{\mathsf{PH}} - R_{\mathsf{PH}}\right)\left(\frac{\partial H_\pi^d}{\partial\langle z\rangle} + \frac{\partial H_r}{\partial\langle z\rangle}\right)\\
&= -\left(\frac{\partial H_\pi^d}{\partial x}\right)^T R_\pi^d\frac{\partial H_\pi^d}{\partial x} - \left(\frac{\partial H_r}{\partial\langle z\rangle}\right)^T R_{\mathsf{PH}}\frac{\partial H_r}{\partial\langle z\rangle} + \left(\frac{\partial H_r}{\partial\langle z\rangle}\right)^T\left(J_{\mathsf{PH}} - R_{\mathsf{PH}}\right)\frac{\partial H_\pi^d}{\partial\langle z\rangle}\,.
\end{aligned}$$

In case we can assure

$$\left(\frac{\partial H_r}{\partial\langle z\rangle}\right)^T\left(J_{\mathsf{PH}} - R_{\mathsf{PH}}\right)\frac{\partial H_\pi^d}{\partial\langle z\rangle} = 0, \tag{78}$$

and $\frac{d}{dt}H_{\mathsf{PH}}^d \le 0$, then, by LaSalle's theorem, the dynamics of the system will converge to the largest invariant set contained in

$$\left\{\langle z\rangle \mid \dot{H}_{\mathsf{PH}}^d = -\left(\partial_x H_\pi^d, \partial_{\langle z\rangle}H_r\right)^T\begin{bmatrix} R_d & 0\\ 0 & R_{\mathsf{PH}}\end{bmatrix}\begin{pmatrix}\partial_x H_\pi^d\\ \partial_{\langle z\rangle}H_r\end{pmatrix} = 0\right\}$$

In particular, we will have local stability of $\langle z\rangle_* = (x_*, 0)$. Observe that at least we have $R_\pi^d \geq 0$, but in general we don't know the character of R_{PH}. In particular, when $R(x) = R \geq 0$ we can assure that $R_{\mathsf{PH}} \geq 0$ and then $\dfrac{d}{dt}H_{\mathsf{PH}}^d \leq 0$.

On the other hand, despite $\dfrac{\partial H_r}{\partial\langle z\rangle}$ and $\dfrac{\partial H_\pi^d}{\partial\langle z\rangle}$ being orthogonal vectors, equation (78) won't be true in general. Its value depends on the expressions of J_{PH} and R_{PH}. In order to guarantee this condition and at least local convergence to the desired equilibrium, one could take more conservative candidates to Lyapunov functions $H^d = H_\pi^d + H_r$ such that $H_{\mathsf{PH}} = H^d + H_r'$.

Example 3.4 (Full-bridge rectifier with a resistive load, revisited) The projection $\mathcal{F}_{(0(2),1(1,R),1(1,I))}$ of Σ_{PH} gives rise to Σ_π defined by

$$H_\pi = \frac{1}{2C}\langle z_2\rangle_0 + \frac{1}{2L}\left(\langle z_1\rangle_1^{R^2} + \langle z_1\rangle_1^{I^2}\right),$$

the matrices

$$J_\pi = \begin{pmatrix} 0 & -2\langle v\rangle_1^R & -2\langle v\rangle_1^I \\ 2\langle v\rangle_1^R & 0 & \omega_0 L \\ 2\langle v\rangle_1^I & -\omega_0 L & 0 \end{pmatrix}, \quad R_\pi = \begin{pmatrix} \frac{4\langle z_2\rangle_0}{R} & 0 & 0 \\ 0 & r & 0 \\ 0 & 0 & r \end{pmatrix},$$

and the forcing term $f_\pi = (0, 0, v_i)^T$.

Designing the system so that $x_* = \left(\frac{C^2V_d^2}{2}, 0, \frac{-LI_d}{2}\right)$ is an asymptotically stable equilibrium of Σ_π, leaded us to choose certain functions $\langle v\rangle_1^R$ and $\langle v\rangle_1^I$ while setting $\langle v\rangle_l = 0\ \forall l \neq 1, -1$. In the higher-dimensional phasor system, this means that the matrix $J_{\mathsf{PH}} - R_{\mathsf{PH}}$ becomes

$$\begin{pmatrix}
-2r & 0 & 0 & 2\langle v\rangle_1^R & 0 & 2\langle v\rangle_1^I & \dots \\
0 & -\frac{4\langle z_2\rangle_0}{R} & -2\langle v\rangle_1^R & -\frac{4\langle z_2\rangle_1^R}{R} & -2\langle v\rangle_1^I & -\frac{4\langle z_2\rangle_1^I}{R} & \dots \\
0 & 2\langle v\rangle_1^R & -r & 0 & \omega_0 L & 0 & \dots \\
-2\langle v\rangle_1^R & -\frac{4\langle z_2\rangle_1^R}{R} & 0 & -\frac{2}{R}\left(\langle z_2\rangle_0 + \langle z_2\rangle_2^R\right) & 0 & -\frac{2\langle z_2\rangle_1^I}{R} & \dots \\
0 & 2\langle v\rangle_1^I & -\omega_0 L & 0 & -r & 0 & \dots \\
-2\langle v\rangle_1^I & -\frac{4\langle z_2\rangle_1^I}{R} & 0 & -\frac{2\langle z_2\rangle_1^I}{R} & 0 & -\frac{2}{R}\left(\langle z_2\rangle_0 + \langle z_2\rangle_2^R\right) & \dots \\
0 & 0 & 0 & \langle v\rangle_1^R & 0 & -\langle v\rangle_1^I & \dots \\
0 & -\frac{4\langle z_2\rangle_2^R}{R} & -\langle v\rangle_1^R & -\frac{2}{R}\left(\langle z_2\rangle_2^R - \langle z_2\rangle_3^R\right) & \langle v\rangle_1^I & \frac{2}{R}\left(\langle z_2\rangle_1^I + \langle z_2\rangle_3^I\right) & \dots \\
0 & 0 & 0 & \langle v\rangle_1^I & 0 & \langle v\rangle_1^R & \dots \\
0 & -\frac{4\langle z_2\rangle_2^I}{R} & -\langle v\rangle_1^I & -\frac{2}{R}\left(\langle z_2\rangle_1^I - \langle z_2\rangle_3^I\right) & -\langle v\rangle_1^R & -\frac{2}{R}\left(\langle z_2\rangle_1^R + \langle z_2\rangle_3^R\right) & \dots \\
0 & 0 & 0 & 0 & 0 & 0 & \dots \\
0 & -\frac{4\langle z_2\rangle_3^R}{R} & 0 & -\frac{2}{R}\left(\langle z_2\rangle_2^R - \langle z_2\rangle_4^R\right) & 0 & \frac{2}{R}\left(\langle z_2\rangle_2^I - \langle z_2\rangle_4^I\right) & \dots \\
\dots & & & & & &
\end{pmatrix}$$

Though $J_{\mathsf{PH}} - R_{\mathsf{PH}}$ has infinite nonzero entries, the ones displayed above are enough to check that (78) is satisfied. Since

$$H_r(\langle z\rangle) = \frac{1}{4L}\langle z_1\rangle_0^2 + \frac{1}{2L}\sum_{k=2}^{\infty}\left(\langle z_1\rangle_k^{R^2} + \langle z_1\rangle_k^{I^2}\right)$$

and $H_\pi^d \equiv H_\pi^d(x)$, we have:

$$\left(\frac{\partial H_r}{\partial\langle z\rangle}\right)^T = \left(\frac{\langle z_1\rangle_0}{2L}, 0, 0, 0, 0, 0, \frac{\langle z_1\rangle_1^R}{L}, 0, \frac{\langle z_1\rangle_2^I}{L}, 0, \frac{\langle z_1\rangle_3^R}{L}, 0, \dots, 0, \frac{\langle z_1\rangle_k^I}{L}, 0, \dots\right),$$

$$\left(\frac{\partial H_\pi^d}{\partial\langle z\rangle}\right)^T = (0, H_1, H_2, 0, H_3, 0, 0, 0, 0, 0, \dots, 0, \dots).$$

Then,

$$\begin{aligned}\left((J_{\mathsf{PH}}-R_{\mathsf{PH}})\frac{\partial H_\pi^d}{\partial\langle z\rangle}\right)^T = \Big(&0,\ -\frac{4\langle z_2\rangle_0}{R}H_1 - 2\langle v\rangle_1^R H_2 - 2\langle v\rangle_1^I H_3,\ 2\langle v\rangle_1^R H_1 - rH_2 + \omega_0 LH_3,\\ &-\frac{4\langle z_2\rangle_1^R}{R}H_1,\ 2\langle v\rangle_1^R H_1 - \omega_0 LH_2 - rH_3, -\frac{4\langle z_2\rangle_1^I}{R}H_1, 0,\\ &-\frac{4\langle z_2\rangle_2^R}{R}H_1 - \langle v\rangle_1^R H_2 + \langle v\rangle_1^I H_3, 0, -\frac{4\langle z_2\rangle_2^I}{R}H_1 - \langle v\rangle_1^I H_2 - \langle v\rangle_1^R H_3, 0,\\ &-\frac{4\langle z_2\rangle_3^R}{R}H_1,\ 0,\ -\frac{4\langle z_2\rangle_3^I}{R}H_1,\ 0,\ \ldots,\ 0,\ -\frac{4\langle z_2\rangle_k^R}{R}H_1,\ 0,\ \ldots\Big)\,,\end{aligned}$$

and therefore

$$\left(\frac{\partial H_r}{\partial\langle z\rangle}\right)^T (J_{\mathsf{PH}}-R_{\mathsf{PH}})\frac{\partial H_\pi^d}{\partial\langle z\rangle} = 0\,.$$

One can also check here that $\left(\dfrac{\partial H_{\mathsf{PH}}}{\partial\langle z\rangle}\right)^T \cdot f_{\mathsf{PH}} = 0$.

Let us study with more detail the expression

$$-\left(\frac{\partial H_\pi^d}{\partial x}\right)^T R_\pi^d \frac{\partial H_\pi^d}{\partial x} - \left(\frac{\partial H_r}{\partial\langle z\rangle}\right)^T R_{\mathsf{PH}}\frac{\partial H_r}{\partial\langle z\rangle}\,.$$

Since $R_\pi^d \geq 0$, we have that $\left(\dfrac{\partial H_\pi^d}{\partial x}\right)^T R_\pi^d \dfrac{\partial H_\pi^d}{\partial x} \geq 0$. In fact, assuming certain hypothesis, it was seen in [10] that the equality holds only when $\pi\langle z\rangle = x_*$. On the other hand,

$$\left(\frac{\partial H_r}{\partial\langle z\rangle}\right)^T R_{\mathsf{PH}}\frac{\partial H_r}{\partial\langle z\rangle} = \frac{r}{2L^2}\langle z_1\rangle_0^2 + \frac{r}{L^2}\sum_{k=2}^{\infty}\left(\langle z_1\rangle_k^{R^2} + \langle z_1\rangle_k^{I^2}\right) \geq 0\,,$$

and the equality is satisfied only when $\langle z_1\rangle_0 = \langle z_1\rangle_k^R = \langle z_1\rangle_k^I = 0$, $\forall k \in \mathbb{N} - \{1\}$. Thus the dynamics of the system will converge to the largest invariant set contained in

$$M = \left\{\langle z\rangle \mid \pi\langle z\rangle = x_*\,,\ \langle z_1\rangle_0 = \langle z_1\rangle_k^R = \langle z_1\rangle_k^I = 0\,,\ \forall k \in \mathbb{N},\ k \neq 1\right\} \tag{79}$$

Let us investigate now what this largest invariant set is. To do that, we need to study the phasor equations for $\langle z_2\rangle_k$, $k \in \mathbb{Z}$, $k \neq 0$. The general expresion of the equations is exactly

$$\frac{d}{dt}\langle z_2\rangle_k = -jk\omega_0\langle z_2\rangle_k - \frac{1}{L}\sum_l \langle v\rangle_{k-l}\langle z_1\rangle_l + \frac{2}{RC}\langle z_2\rangle_k\,.$$

In particular, the invariant dynamics satifies

$$\sum_l \langle v\rangle_{k-l}\langle z_1\rangle_l = \langle v\rangle_{k-1}\langle z_1\rangle_1 + \langle v\rangle_{k+1}\langle z_1\rangle_{-1}\,.$$

Moreover, since we are taking $\langle v\rangle_l \neq 0$ only for $l = 1, -1$, the real and imaginary parts of the $\langle z_2\rangle_k$ equation for $k \neq 0,\ 2$ can be written as

$$\begin{cases}\dfrac{d}{dt}\langle z_2\rangle_k^R &= k\omega_0\langle z_2\rangle_k^I - \dfrac{2}{RC}\langle z_2\rangle_k^R\,,\\ \dfrac{d}{dt}\langle z_2\rangle_k^I &= -k\omega_0\langle z_2\rangle_k^R - \dfrac{2}{RC}\langle z_2\rangle_k^I\,,\end{cases}$$

In other words, for each k this system is of the form

$$\dot{y} = \begin{pmatrix} \frac{-2}{RC} & k\omega_0 \\ -k\omega_0 & \frac{-2}{RC}\end{pmatrix} y\,.$$

Now, as $\frac{-2}{RC} \neq 0$, $(\langle z_2\rangle_{k,*}^R, \langle z_2\rangle_{k,*}^I) = (0,0)$ is an asymptotically stable equilibrium for eack k system, $k \neq 0,\ 2$ and the invariant set contained in M in necessarily within

$$E = \{\langle z\rangle \mid \pi\langle z\rangle = x_*\,,\ \langle z_1\rangle_0 = \langle z_1\rangle_k = \langle z_2\rangle_l = 0\,,\ \forall k,\ l \in \mathbb{Z}\ k \neq 1\,, l \neq 2,\ 0\}$$

In terms of the original system Σ, this means we have asymptotic convergence to the set of trajectories

$$z_{1,*}(t) = LI_d \sin(\omega_0 t)\,, \qquad z_{2,*}(t) = \frac{C^2V_d^2}{2} + \beta_{z_2}\sin(2\omega_0 t + \theta_{z_2})\,.$$

Now, if C is chosen so that there is a low voltage in the capacitor, then β_{z_2} can be neglected with respect to $\frac{C^2V_d^2}{2}$, and we are practically achieving global asymptotic convergence to the desired trajectory

$$z_{1,*}(t) = LI_d \sin(\omega_0 t)\,, \qquad z_{2,*}(t) = \frac{C^2V_d^2}{2}\,.$$

Remark 3.5 For the most general model of the full-bridge rectifier, all computations can be reproduced until expression (79). From then on, a detailed analysis of the phasor equations is needed to reduce the invariant set to E. In any case, the desired equilibrium $(x_*, 0)$ is guaranteed to be locally stable by this procedure.

References

[1] D. Biel, E. Fossas, F. Guinjoan, and R. Ramos. Sliding mode control of a boost-buck converter for ac signal tracking task. *Proceedings of ISCAS'99. Orlando*, pages 242–245, 1999.

[2] H. Bühler. *Réglage par mode de glissement*. Presses Polytechniques Romandes, 1986.

[3] V.A. Caliscan, G.C. Verghese, and A.M. Stankovic. Multi-frequency averaging of dc/dc converters. *IEEE Transactions on Power Electronics*, 14(1):124–133, January 1999.

[4] M. Carpita, M. Marchesioni, M. Oberti, and L. Puguisi. Power conditioning system using sliding mode control. *Proceedings PESC 1988*, pages 623–633, 1988.

[5] R.A. De Carlo, S.H. Zak, and G.P. Matthews. Variable structure control of nonlinear multivariable systems: A tutorial. *Proceedings IEEE*, 76(3):212–232, 1988.

[6] A.F. Filipov. Differential equations with discontinuous right-hand sides. *American Mathematical Society Translations*, 42:199–231, 1964.

[7] E. Fossas and D. Biel. A sliding mode approach to robust generation on dc-to-dc converters. *Conf. on Dec. and Control. Kobe, Japan*, pages 4010–4012, 1996.

[8] E. Fossas, D. Biel, R. Ramos, and A. Sudriá. Programmable logic device applied to the quasi-sliding control implementation based on zero averaged dynamic. *40th IEEE Conference on Decision and Control (CDC'01). Orlando, Florida (USA)*, pages 1825–1830, 2001.

[9] E. Fossas, R. Griñó, and D. Biel. *Quasi-Sliding control based on pulse width modulation, zero averaged dynamics and the L2 norm*, pages 335–344. World Scientific, Singapur, 2001.

[10] C. Gaviria, E. Fossas, and R. Griñó. Robust controller for a full-bridge rectifier using the ida-pbc approach and gssa modelling. *Submitted to IEEE Trans. Circuits and Systems*, 2003.

[11] J. Jung, S. Lim, and K. Nam. A feedback linearizing control scheme for a pwm converter-inverter having very small dc-link capacitor. *Trans. Ind. Applicat.*, 35:1124–1131, Sep/Oct 1999.

[12] J. Mahdavi, A. Emaadi, M. D. Bellar, and M. Ehsani. Analysis of power electronic converters using the generalized state-space averaging approach. *IEEE Transactions on Circuits and Systems I*, 44(8):767–770, August 1997.

[13] L. Malesani, L. Rossetto, G. Spiazzi, and A. Zuccato. An ac power supply with sliding-mode control. *IEEE Industry Applications Magazine*, pages 32–38, 1996.

[14] L.M. Malesani, L. Rossetto, and P. Tomasin. AC/DC/AC pwm converter with reduced energy stored in the dc link. *IEEE Trans. Ind. Applications*, 31:287–292, 1995.

[15] B. Nicolas, M. Fadel, and Y. Chéron. Sliding mode control of dc-to-dc converters with input filter based on the lyapunov-function approach. *Proceedings of European Power Electronics Conference (EPE)*, pages 1338–1343, 1995.

[16] H. Pinheiro, A.S. Martins, and J.R. Pinheiro. A sliding mode controller in single phase voltage source inverters. *International Conference on Industrial Electronics Control and Instrumentation (IECON)*, pages 394–398, 1994.

[17] J.M. Ruiz, S. Lorenzo, I. Lobo, and J. Amigo. Minimal ups structure with sliding mode control and adaptive hysteresis band. *Proceedings of International Conference on Industrial Electronics Control and Instrumentation (IECON)*, pages 1063–1067, 1990.

[18] S.R. Sanders, J.M. Noworolski, X.Z. Liu, and G.C. Verghese. Generalized averaging method for power conversion circuits. *IEEE Transactions on Power Electronics*, 6(2):251–259, April 1991.

[19] J.F. Silva and S.S. Paulo. Fixed frequency sliding modulator for current mode pwm inverters. *Proceedings of Power Electronic Specialist Conference (PESC)*, pages 623–629, 1993.

[20] H. Sira-Ramírez. Sliding motions in bilinear switched networks. *IEEE Trans. on Circuits and Systems*, 34(8):919– 933, August 1987.

[21] H. Sira-Ramírez. Differential geometric methods in variable structure control. *Int. J. Control*, 48:1359–1390, 1988.

[22] G. Tadmor. On approximate phasor models in dissipative bilinear systems. *IEEE Trans. on Circuits and Systems I*, 49:1167–1179, 2002.

[23] V.I. Utkin. *Sliding Modes and their Application in Variable Structure Systems*. Mir, 1978.

[24] R. Venkataramanan, A. Sabanovic, and S. Čuk. Sliding mode control of dc-to-dc converters. *Proceedings IECON 1985*, pages 251– 258, 1985.

[25] K.D. Young, V.I. Utkin, and Ü. Özgüner. A control engineerr's guide to sliding mode control. *Proceedings of IEEE Workshop on Variable Structure Systems*, pages 1–14, 1996.